

Berry's phase and quantum dynamics of ferromagnetic solitons

Hans-Benjamin Braun and Daniel Loss

Department of Physics, Simon Fraser University, Burnaby, British Columbia, Canada V5A 1S6

(Received 31 May 1995)

We study spin parity effects and the quantum propagation of solitons (Bloch walls) in quasi-one-dimensional ferromagnets. Within a coherent state path integral approach we derive a quantum field theory for nonuniform spin configurations. The effective action for the soliton position is shown to contain a gauge potential due to the Berry phase and a damping term caused by the interaction between soliton and spin waves. For temperatures below the anisotropy gap this dissipation reduces to a pure soliton mass renormalization. The quantum dynamics of the soliton in a periodic lattice or pinning potential reveals remarkable consequences of the Berry phase. For half-integer spin, destructive interference between opposite chiralities suppresses nearest-neighbor hopping. Thus the Brillouin zone is halved, and for small mixing of the chiralities the dispersion reveals a surprising dynamical correlation: Two subsequent band minima belong to different chirality states of the soliton. For integer spin the Berry phase is inoperative and a simple tight-binding dispersion is obtained. Finally it is shown that external fields can be used to interpolate continuously between the Bloch wall dispersions for half-integer and integer spin.

I. INTRODUCTION

Quantum effects in low-dimensional magnetism are a fascinating subject which has attracted much interest over the years. A notable example is antiferromagnetic chains where the quantum spin (or Berry¹) phase leads to remarkable parity effects. It is for integer spin S only that the ground state exhibits an excitation (or Haldane²) gap whereas for half-odd-integral S such gaps are suppressed by interfering Berry phases.³ Related to this phenomenon is the suppression of mesoscopic stiffness fluctuations for S half-integral antiferromagnets, whereas such fluctuations grow with chain size for integer S (similar to universal conductance fluctuations in mesoscopic metals).⁴

Over recent years, the rapid advances in nanostructure technology⁵ have opened the door to another class of magnetic systems: small single domain particles that display striking mesoscopic quantum phenomena⁶ (MQP) such as quantum coherence, quantum tunneling, or spin parity effects. These particles exhibit one or several directions of minimal anisotropy energy between which the spins can tunnel coherently. Motivated by theoretical predictions for uniform ferromagnets⁷⁻¹⁰ and antiferromagnets¹¹ several experiments at subkelvin temperatures have shown either temperature-independent relaxation phenomena¹²⁻¹⁴ or a well-defined resonance¹⁵ (in the ac susceptibility) which scales exponentially with the number of spins¹⁶ in accordance with theory.¹¹ Although these observations have been criticized on the basis of dissipation models, such as the influence of nuclear spins,¹⁷ the experiments on antiferromagnetic ferritin¹⁵ provide a strong indication that the spins indeed tunnel coherently at low temperatures.

In subsequent work, it has been shown¹⁸⁻²¹ that also tunneling depends on the spin parity via Berry phases, and that magnetization switching is allowed only if the total spin of the particle is integral, but not otherwise. Similar results have been found in uniform antiferromagnetic particles.^{18,20,22,23}

While such spin parity effects are sometimes related to

Kramers degeneracy, in particular in single domain ferromagnets,^{7,8,18} they typically go beyond this theorem in rather unexpected ways.^{18,21} It is notably for *nonuniform* magnets that such effects can be quite intriguing, as we know since Haldane's work on antiferromagnets.² On the other hand, there has not been much related study on nonuniform ferromagnets, primarily because their ground state is trivial and did not seem to offer much room for surprises. However, this is by no means so, and it is one of our goals to show that ferromagnets with more than one magnetic domain do exhibit interesting spin parity effects and that these effects have experimental consequences.

We address the issue of spin parity in the context of MQP, although the Berry phase effects discussed here are of general relevance in low-dimensional magnetism. We start by considering the coherent quantum propagation of Bloch walls in the presence of periodic pinning potentials. Such potentials are naturally provided by the underlying crystal lattice or some superlattice structure that can be created by periodic deposition of materials with different anisotropies.^{24,21,25} Parenthetically we note that periodic pinning provides a much smaller barrier height and tunneling distance than one isolated pinning center would do. Thus the tunneling probability will be drastically enhanced in this case^{24,21} compared to the more traditional scenario where experiment^{26,27,13} and theory²⁸⁻³² focus on wall tunneling out of single pinning centers.

In a collective coordinate description the Bloch wall is then seen to behave like a single degree of freedom moving in a periodic structure.²⁴ This in turn results in characteristic Bloch bands in reciprocal space, where the bandwidth is determined by the tunneling rate through the potential. It is now at this stage where the Berry phase enters the wall dynamics via an effective gauge potential that depends on the *chirality*, i.e., the internal rotation sense of the Bloch wall. For half-integer spins this gauge potential induces a halving of the associated Brillouin zone. At the same time a remarkable dynamical correlation occurs: Two subsequent band

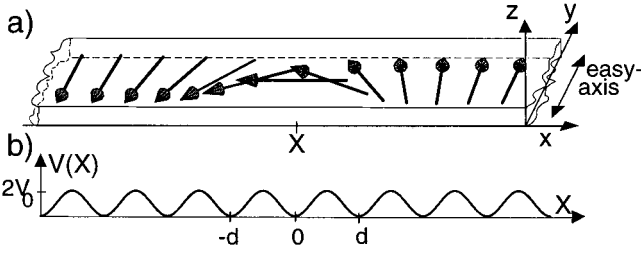


FIG. 1. (a) Bloch wall configuration with $Q=1$, $C=-1$ in a thin long slab centered at the pinning site $X=0$; (b) periodic pinning potential V for the wall center X .

minima belong to opposite chiralities. Thus the chirality of the wall alternates when the system is adiabatically driven through the Brillouin zones by an external magnetic field. As we shall argue, this phenomenon can be experimentally observed if there is a finite tunneling probability between the chiralities, a condition which is not difficult to meet in real systems. Due to the topological nature of the Berry phase these results are independent of details such as the shape of the soliton and the pinning potential. Thus we expect that band halving and chirality correlation also occur in the limit of a spin-1/2 chain where the soliton width approaches one lattice constant.

Besides these spin parity effects, the band structure leads to interesting coherence effects in the form of Bloch oscillations of the wall center.^{24,21} As a result the sample magnetization oscillates in response to a *static* magnetic field, a behavior which is very similar to the ac-Josephson effect in superconductors.

In principle these results hold for an arbitrary number N_A of coupled ferromagnetic chains. However, observation of MQP becomes increasingly difficult with increasing N_A since observability requires tunneling exponents (which grow with N_A) to be of the order of Planck's constant. This necessarily limits the size of sample cross sections (but not their lengths) and restricts considerations to low-dimensional ferromagnets, most typically of quasi-one-dimensional size. An important consequence of this reduced dimensionality is the fact that dissipation due to spin waves has a negligible effect on the wall dynamics since there is an associated finite size gap (besides the anisotropy gap) in the spin wave spectrum. It is due to these gaps that at temperatures typically below 100 mK the spin waves freeze out exponentially fast, and are thus simply irrelevant for dissipation (they only lead to a minor soliton mass renormalization as we shall show explicitly).

To simplify our discussion we consider in the following the limit of large hard-axis anisotropy^{33,34} as it occurs, for instance, in an yttrium iron garnet (YIG) sample of the shape shown in Fig. 1. We can then eliminate the out-of-easy-plane degree of freedom and the spin model reduces to that of a sine-Gordon model plus a gauge term coming from the Berry phases. In a quantum field approach we introduce collective coordinates, eliminate the spin waves, and arrive at an effective action for the wall position. The spin waves give rise to a nonlocal term in the action which can be cast into the well-known Caldeira-Leggett form at low temperatures. In this way we make contact with phenomenological formula-

tions of dissipation^{35,36} as extensively discussed in the context of MQP,³⁷ and show that the spectral function has a gap due to anisotropies. While there have been a number of works in various contexts related to intrinsic soliton damping,^{38-42,30} we believe that the approach presented here is most adequate to the combined description of wall dynamics and Berry phases and, moreover, provides the first complete discussion of spin wave dissipation, particularly in the context of MQP. Finally we note that a brief account of part of the results presented here has been given before.^{24,21}

The outline of the paper is as follows. In Sec. II we discuss the derivation of the spin action plus topological phase from the Heisenberg model. Details of this derivation via coherent spin states together with a unified treatment of the Berry phase in different gauges are given in Appendix A. In Sec. III we discuss static Bloch wall solutions and derive the sine-Gordon action plus gauge term in Sec. IV. To gain confidence in our approach we first consider the uniform limit and show that this gauge term reproduces the known spin parity behavior.¹⁸ As a by-product we also obtain the tunneling prefactor. In Sec. V we discuss the coupling between Bloch wall and spin waves and show that spin wave dissipation is negligible at low temperatures, technical details are presented in Appendix B. In Sec. VI we discuss the influence of the Berry phase on the Bloch wall dynamics in a periodic potential, first in the nearly free (Sec. VI B) and then in the tight-binding limit (Sec. VI C). In both cases it is shown that for half-integral spin the Brillouin zone is halved and the chirality alternates. Experimental implications are given in Sec. VII, where we also give results for the level splitting due to the tunneling between the two wall chiralities. Finally in Sec. VIII we discuss how the interference effects are altered by external fields. A note regarding the terminology: the terms soliton and Bloch (or domain) wall are used interchangeably to denote the transition region between domains in ferromagnets.

II. MODEL

In this section we derive a continuum field theory to describe the quantum dynamics of nonuniform spin configurations in ferromagnets. Our starting point is a microscopic Heisenberg spin Hamiltonian with local anisotropies. The transition amplitude between two nonuniform spin configurations is then expressed as a coherent state path integral. The corresponding action differs from the classical micromagnetic expression by a total derivative.^{18,21,24} While this term does not affect the classical equations of motion, it gives rise to quantum mechanical interference effects and thus leads in a natural way to the quantization of micromagnetics. Several examples of such interference effects will be discussed below in Secs. IV and VI-VIII.

Ferromagnetic insulators can often be described by a Heisenberg Hamiltonian with anisotropies

$$\mathcal{H} = -\tilde{J} \sum_{i,\rho} \mathbf{S}_i \cdot \mathbf{S}_{i+\rho} - \tilde{K}_y \sum_i (S_i^y)^2 + \tilde{K}_z \sum_i (S_i^z)^2, \quad (2.1)$$

where \mathbf{S}_i denotes the spin operator at the lattice site i . For simplicity we assume that the spins form a simple cubic lattice of lattice constant a . Throughout this work we shall use units such that $\hbar = 1$. The first term on the right-hand side

(RHS) of (2.1) is the exchange interaction between a spin at the lattice site i and its nearest neighbors at the lattice sites $i+\rho$. The next term is an easy-axis anisotropy along the y axis with anisotropy constant $\tilde{K}_y > 0$. The third term is a hard-axis anisotropy of strength $\tilde{K}_z > 0$ which renders the xy plane an easy plane. The spins will thus preferably point parallel or antiparallel to the y axis.

The anisotropies that are used in (2.1) are effective anisotropies and may arise from two different microscopic mechanisms. One contribution is the magnetocrystalline anisotropy which is due to the interaction of the magnetic moments with their neighboring atoms via spin-orbit interaction. Consequently this contribution reflects the symmetry of the crystal lattice. The second contribution is the dipolar interaction between the magnetic moments. Due to its long range nature this contribution depends on the sample shape and is in general a nonlocal functional of the magnetization configuration. It is this magnetostatic interaction that gives rise to the existence of domains in macroscopic samples. However, for quasi-one-dimensional configurations this interaction considerably simplifies and can be modeled by local anisotropies as in (2.1).⁴³

Our focus in this work will be on elongated samples as shown in Fig. 1 with transverse dimensions smaller than the length scale $a[\tilde{J}/\tilde{K}_z]^{1/2}$. Spin waves running transverse to the sample^{38,44} then exhibit a finite size gap such that they are frozen out at low temperatures.⁴⁵ This condition is met in most experimental situations studied so far and thus we shall use a quasi-one-dimensional model in the following. Truly three-dimensional samples where all degrees of freedom are allowed to be excited are of rather limited interest for MQP since their tunneling rates *and* associated crossover temperatures (separating the classical from the quantum regime) are in general too small to be observed.²¹

We now turn to the path integral formulation of the system described by the Hamiltonian (2.1). We introduce coherent spin states⁴⁶ at each lattice site, defined by $\mathbf{\Omega}_i \cdot \mathbf{S}_i |\mathbf{\Omega}_i\rangle = S |\mathbf{\Omega}_i\rangle$ where $\mathbf{\Omega} = (\sin\theta \cos\phi, \sin\theta \phi, \cos\theta)$ is a unit vector. The whole system is then described by a product of coherent states at each of the N_L lattice sites, i.e., $|\{\mathbf{\Omega}\}\rangle = \otimes_{i=1}^{N_L} |\mathbf{\Omega}_i\rangle$. Since we are interested in configurations that are varying slowly compared to the lattice constant, the spin state can be described by a smoothly varying unit vector field $\mathbf{\Omega}(x, \tau)$ depending on the coordinate x along the sample and the imaginary time τ . As outlined in Appendix A, the transition amplitude between the two states $|\{\mathbf{\Omega}_a\}\rangle$ and $|\{\mathbf{\Omega}_b\}\rangle$ can then be expressed as an (imaginary) time path integral

$$\langle\{\mathbf{\Omega}_b\}|e^{-\beta\mathcal{H}}|\{\mathbf{\Omega}_a\}\rangle = \int \mathcal{D}\phi \mathcal{D}(\cos\theta) e^{-\mathcal{S}_E[\phi, \theta]}, \quad (2.2)$$

where the integration is over all configurations that satisfy the boundary conditions $\mathbf{\Omega}(x, 0) = \mathbf{\Omega}_a(x)$ and $\mathbf{\Omega}(x, \beta) = \mathbf{\Omega}_b(x)$ (spatial boundary conditions will be specified later). The Euclidean action is given by

$$\mathcal{S}_E = \mathcal{S}_{\text{WZ}} + \int_0^\beta d\tau H, \quad (2.3)$$

with the Wess-Zumino or Berry phase term

$$\mathcal{S}_{\text{WZ}} = i \frac{SN_A}{a} \int_0^\beta d\tau \int_{-L/2}^{L/2} dx \dot{\phi} (1 - \cos\theta), \quad (2.4)$$

with $\dot{\phi} = \partial_\tau \phi$ and where a gauge has been chosen with the coherent states underlying the path integral (2.2) expressed in the ‘‘north-pole’’ parametrization (cf. Appendix A). Equation (2.4) has for closed trajectories the form of the sum over the Berry phases of all $N_A L/a$ spins. The energy is given by

$$H = N_A \int_{-L/2}^{L/2} dx \{J[(\partial_x \theta)^2 + \sin^2 \theta (\partial_x \phi)^2] - K_y [\sin^2 \theta \sin^2 \phi - 1] + K_z \cos^2 \theta\}. \quad (2.5)$$

N_A denotes the number of spins in the cross sectional area \mathcal{A} of the sample, and L is the sample length. The parameters in (2.5) are related to those in (2.1) via

$$J = \tilde{J} S^2 a, \quad K_{y,z} = \tilde{K}_{y,z} S^2 / a. \quad (2.6)$$

The energy (2.5) is identical to the traditional micromagnetic energy expression.^{43,47–49} J and $K_{y,z}$ can now be related to the micromagnetic anisotropy and exchange constants $J = Aa^2$, $K_y = K_e a^2$, and $K_z = K_h a^2$. For an elongated slab as shown in Fig. 1, we have $K_e = K_{e,\text{cryst}}$ and $K_h = K_{h,\text{cryst}} + 2\pi M_0^2$, where $M_0 = g\mu_B S/a^3$ is the saturation magnetization, and $K_{e,\text{cryst}}$, $K_{h,\text{cryst}}$ describe crystalline anisotropies. Note, however, that for other sample geometries the demagnetizing term enters in a different form. For instance, for a cylindrical wire we would have $K_e = K_{e,\text{cryst}} + \pi M_0^2$, while the hard-axis anisotropy would be of purely crystalline origin. (For other examples see Fig. 8 of Ref. 43.) The demagnetizing energy is not always important; in particular, for samples with misoriented anisotropy axes (see p. 15 of Ref. 47) the crystalline anisotropies can be much larger than $2\pi M_0^2$.

In saddle point approximation, $\delta\mathcal{S}_E = 0$, and rotating to real time $t = -i\tau$, we recover the classical Landau-Lifshitz equations of motion

$$\sin\theta \partial_t \phi = -\frac{a}{S} \frac{\delta H}{\delta \theta}, \quad \partial_t \theta = \frac{a}{S} \frac{1}{\sin\theta} \frac{\delta H}{\delta \phi}. \quad (2.7)$$

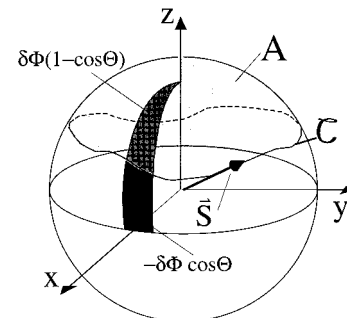


FIG. 2. The Berry phase factor for one single spin \mathbf{S} , $\exp\{iS \int d\phi (1 - \cos\theta)\} = e^{iSA}$, where A is the area on the unit sphere enclosed by the trajectory \mathcal{C} traced out by \mathbf{S} .

These classical equations are not affected by the total derivative $\dot{\phi}$ in (2.4) and thus follow from the classical Lagrangian density⁴⁸ $\mathcal{L} = -(SN_A/a)\partial_t\phi \cos\theta + H$.

Note, however, that the $\dot{\phi}$ term is of crucial importance for the quantum dynamics: While the path integral (2.2) contains higher-winding-number contributions where a path retraces itself, the Wess-Zumino term enforces quantization by destructive interference of paths which do not satisfy the condition $S\sum_i A_i = 2\pi n$, where A_i is the area enclosed by the trajectory of the i th spin on the unit sphere cf. Fig. 2. If the $\dot{\phi}$ term were dropped in (2.4) — a “gauge” that has sometimes been used in the literature — the area A_i would be measured with respect to the equator and one would have to impose the additional constraint⁵⁰ that the paths not intersect the “dateline.” This constraint is very difficult to handle within a path integral formalism. On the other hand, ignoring this constraint would lead to a wrong semiclassical quantization of half-integral spins. Moreover, one would not obtain the suppression of tunneling for half-integer spins in small ferromagnetic particles,¹⁸ in clear contradiction to Kramers theorem which requires that the ground state not be split. In Appendix A we show that all these difficulties can be avoided if one starts from one single premise — the single valuedness of the coherent states — which leads to a restricted set of “admissible” gauges.

Finally, we remark that if we work in the south-pole parametrization of the coherent state [cf. (A2)], the $\dot{\phi}$ term in (2.4) changes sign but, of course, all physical effects that will be derived below are independent of the gauge (provided the gauge is admissible).

III. BLOCH WALL CONFIGURATIONS

There are two energetically degenerate spin configurations which minimize the energy (2.1): uniform configurations with all spins pointing either along the positive or along the negative y direction. We are now interested in structures that interpolate between these two configurations. Due to the easy-axis anisotropy in (2.1), this transition region will have a finite width and form a Bloch wall (or soliton). Such Bloch walls may have various origins in realistic samples. They can simply be enforced by keeping the spins at both sample ends antiparallel to each other. For certain sample geometries, their existence can be favored by long range magnetostatic interactions which have not been built into (2.5). Finally, in strictly one-dimensional chains, solitons with width of one lattice constant rather than spin waves can form the elementary excitations.^{51,52}

A static Bloch wall connects the anisotropy minima $\phi = \pm\pi/2$ within the easy plane $\theta = \pi/2$ and thus satisfies the Euler-Lagrange equations

$$J\partial_x^2\phi + K_y \sin\phi \cos\phi = 0. \quad (3.1)$$

With the additional condition $\partial_x\phi(\pm\infty) = 0$, this can be immediately integrated once

$$\frac{J}{K_y}(\partial_x\phi)^2 - \cos^2\phi = 0. \quad (3.2)$$

This equation exhibits the symmetries $\phi \rightarrow -\phi$ and $\phi \rightarrow \phi + \pi$, which reflect the fact that the energy (2.1) is

invariant under rotations by π around each axis in spin space. Consequently, there are four different Bloch wall solutions of (3.2) (see, e.g., Ref. 47):

$$\phi_{QC}(x) = -QC\frac{\pi}{2} + 2 \arctan e^{Cx/\delta}, \quad \theta = \frac{\pi}{2}, \quad (3.3)$$

of width $\delta = \sqrt{J/K_y}$. In order to distinguish the four different soliton configurations we have introduced the “charge” $Q = (1/2)\int dx \partial_x(\sin\phi)$ and the “chirality”

$$C = \frac{1}{\pi} \int_{-\infty}^{\infty} dx \partial_x\phi \quad (3.4)$$

of a spin configuration. For the Bloch walls (3.3) we have $Q, C = \pm 1$, and all four walls have the same energy,

$$E_0 = 2JN_A \int_{-\infty}^{\infty} dx (\partial_x\phi_{QC})^2 = 4N_A \sqrt{JK_y}. \quad (3.5)$$

The definition of the chirality C simply tells us whether the angle ϕ increases or decreases as we proceed in the positive x direction along the sample. The definition of the charge Q is motivated by the response of the Bloch wall to an applied magnetic field: For an external field along the positive y axis, a Bloch wall of positive charge moves along the positive x axis while a negatively charged wall moves in the opposite direction. (We recall that the spin is antiparallel to the magnetization.) Within the present description, the spin is allowed to point into an arbitrary direction on the unit sphere S^2 . In this case, only the charge is a topological invariant, i.e., for infinite sample length field configurations of opposite charge cannot be deformed into each other without overcoming an infinite energy barrier. Solitons of different chirality (but the same charge) can be deformed into each other via a “Néel wall” configuration where the spin at the wall center points along the hard axis. It is only in the XY limit of large hard-axis anisotropy where the configuration space of the spins becomes a circle and the chirality also becomes a topological invariant. It will be this limit that shall be considered in the next section, but we shall return to the general case when we discuss chirality tunneling in Sec. VII.

IV. RELATION TO THE SINE-GORDON MODEL

In some materials such as elongated YIG films (cf. Fig. 2) or in garnet crystals with misoriented anisotropy axes, the hard-axis anisotropy is much larger than the easy-axis anisotropy, typically by a factor of 10 or more. As a consequence, deviations away from the easy plane become energetically costly and the magnetization will be confined to the easy plane and the system can effectively be described in the easy-plane variable ϕ only.

In the limit $K_z \gg K_y$, deviations away from the easy plane are suppressed and we can expand⁵³

$$\theta(x, \tau) = \pi/2 - \vartheta(x, \tau), \quad (4.1)$$

where $|\vartheta| \ll 1$. Inserting (4.1) into the action (2.4) we obtain up to second order in ϑ

$$\mathcal{S}_E = N_A \int dx d\tau \left\{ i \frac{S}{a} \partial_\tau \phi + J (\partial_x \phi)^2 + K_y \cos^2 \phi - i \frac{S}{a} \vartheta \partial_\tau \phi + \vartheta \mathcal{L} \vartheta \right\}, \quad (4.2)$$

where $\mathcal{L} = -J \partial_x^2 - J (\partial_x \phi)^2 + K_y \sin^2 \phi + K_z$. If the fluctuations in both ϑ and ϕ have wavelength λ larger than the domain wall width, $\lambda \gg \delta$, the hard-axis anisotropy becomes dominant and $\mathcal{L} = K_z + O(K_y/K_z)$. With this approximation, we insert (4.1) into (2.2) and using $\mathcal{D} \cos \theta \approx \mathcal{D} \vartheta$ we can perform the Gaussian integrations. The transition amplitude can then be expressed as a path integral over the azimuthal angle ϕ alone,

$$\langle \{ \Omega_b \} | e^{-\beta \mathcal{H}} | \{ \Omega_a \} \rangle = \int \mathcal{D}\phi e^{-\mathcal{S}_{\text{SG}}[\phi]}, \quad (4.3)$$

with the boundary conditions $\phi(x, 0) = \phi_a(x)$, and $\phi(x, \beta) = \phi_b(x)$. The action has the following form:

$$\mathcal{S}_{\text{SG}} = N_A \int dx d\tau \left\{ i \frac{S}{a} \partial_\tau \phi + J \left[\frac{1}{c^2} (\partial_\tau \phi)^2 + (\partial_x \phi)^2 \right] + K_y \cos^2 \phi \right\}, \quad (4.4)$$

where we have introduced the asymptotic spin wave velocity

$$c = (2a/S) \sqrt{JK_z}. \quad (4.5)$$

We thus have arrived at the important result that *for large hard-axis anisotropy the dynamics of a mesoscopic ferromagnet is described by the sine-Gordon (SG) action plus a topological term* $iSN_A \int (dx/a) \int d\tau \dot{\phi}$. While the reduction to the sine-Gordon model has been known for some time,^{54,9,51} the topological term has not been identified before. This term is of central importance for the quantization of the spin system as we shall see below. It is this term that is responsible for observable effects such as band halving and chirality correlation.

We can now explicitly verify the consistency of our approach. \mathcal{S}_{SG} has the same long wavelength excitations as the full magnetic model described by the action (2.3). In the latter model, deviations from the uniform state $\phi = \pi/2$, $\theta = \pi/2$ along the easy axis have the spin-wave spectrum $\omega_k = 2(a/S) ([Jk^2 + K_y + K_z][Jk^2 + K_y])^{1/2}$, with k the spin-wave wave vector.⁵⁵ For $K_z \gg K_y$ and $k < \sqrt{K_z}/J$ this reduces to $\omega_k = 2(a/S)(K_z[Jk^2 + K_y])^{1/2} = c \sqrt{k^2 + \delta^{-2}}$ which is identical to the spin wave spectrum in the sine-Gordon model (4.4) around $\phi = \pi/2$. Similarly, the dynamic soliton solutions of the spin system (see, e.g., Ref. 56) which correspond to moving Bloch walls have their counterpart in the SG model in this limit. Even soliton-antisoliton breather solutions of the spin system have analogues in SG breather solutions.⁵⁷ This is surprising since in the spin model breathers exhibit a precession around the easy axis and thus do not stay close to the easy plane as required in (4.1). The connection between the spin model and the SG system is therefore more general than the above derivation suggests.

A. Spin tunneling for $K_z \gg K_y$

To illustrate the importance of the topological term derived above, we consider the case of a uniform spin configuration as, e.g., realized in a nanoscale ferromagnetic particle. We shall show that the reduced model (4.4) reproduces both the spin parity effect¹⁸ and the tunneling action⁹ of the full magnetic model in the XY limit. In addition we shall also evaluate the prefactor of the transition amplitude resulting from Gaussian fluctuations around the instanton path.

For uniform configurations $\phi = \phi(\tau)$, the action (4.4) reduces to

$$\tilde{\mathcal{S}}_{\text{SG}} = N \int d\tau \left\{ iS \partial_\tau \phi + \frac{Ja}{c^2} (\partial_\tau \phi)^2 + K_y a \cos^2 \phi \right\}, \quad (4.6)$$

where $N = N_A L/a$ is the total number of spins in the sample. Note that ϕ describes the azimuthal angle of a spin and is a compact variable ($\phi + 2\pi$ is identified with ϕ). The tunneling amplitude between the anisotropy minima at $\phi = \pm \pi/2$ is then given by

$$\left\langle \phi = \frac{\pi}{2} \left| e^{-\beta \mathcal{H}} \right| \phi = -\frac{\pi}{2} \right\rangle = \int_{\phi(0) = -\pi/2}^{\phi(\beta) = \pi/2} \mathcal{D}\phi e^{-\tilde{\mathcal{S}}_{\text{SG}}[\phi]}. \quad (4.7)$$

The dominant contributions to the transition amplitude are the extrema of the action which satisfy $\delta \tilde{\mathcal{S}}_{\text{SG}} = 0$ or

$$(J/c^2) \partial_\tau^2 \phi + K_y \sin \phi \cos \phi = 0. \quad (4.8)$$

Note that this equation is formally equivalent to (3.1). Similarly, as a consequence of the symmetry of the action (4.4) under π rotations around the hard axis, i.e., $\phi \rightarrow \phi + \pi$, the two anisotropy minima can be connected by two different paths. These ‘‘instanton’’ and ‘‘anti-instanton’’ trajectories are given by $\phi_\pm(\tau) = -\pi/2 \pm 2 \arctan e^{\omega_I(\tau - \tau_0)}$ and describe a transition from $\phi = -\pi/2$ to $\pi/2$ in the clockwise (ϕ_+) or anticlockwise direction (ϕ_-). The transition occurs at τ_0 within a finite imaginary time interval characterized by the ‘‘instanton frequency’’ $\omega_I = c/\delta = (2a/S) \sqrt{K_y K_z}$. Inserting ϕ_\pm into the action (4.6), we recognize that the topological term gives rise to a phase which differs in sign for instantons or anti-instantons,

$$\tilde{\mathcal{S}}_{\text{SG}}[\phi_\pm] = \pm i \pi N S + \mathcal{S}_0, \quad (4.9)$$

with the tunneling exponent⁵⁸ $\mathcal{S}_0 = 2NS \sqrt{K_y/K_z}$.

The effect of the topological phase may now be seen as follows. Adding the contributions of one single instanton and anti-instanton to the action, we obtain with (4.9) for (4.7)

$$\begin{aligned} \left\langle \phi = \frac{\pi}{2} \left| e^{-\beta \mathcal{H}} \right| \phi = -\frac{\pi}{2} \right\rangle &\propto \sum_{\sigma = \pm 1} e^{-\tilde{\mathcal{S}}_{\text{SG}}[\phi_\sigma]} \\ &= 2 \cos(\pi N S) e^{-\mathcal{S}_0}. \end{aligned} \quad (4.10)$$

Thus the transition amplitude vanishes for half-odd-integer NS since tunneling paths of opposite winding (or ‘‘chirality’’) interfere destructively with each other. A calculation within the ‘‘dilute instanton gas’’ approximation⁵⁹ reveals that this interference persists to all orders in the instanton contributions. Identifying $\mu = 2NJa/c^2 = NS^2/2K_z a$,

$\kappa = NK_y a$, $\alpha = -NS$, and $d = \pi$ we obtain (including the contributions of Gaussian fluctuations around the instanton)

$$\left\langle \frac{\pi}{2} \left| e^{-\beta \mathcal{H}} \right| - \frac{\pi}{2} \right\rangle \propto e^{-\beta \omega_l/2} \sinh \left(\beta \frac{\Delta}{2} \cos(NS\pi) \right) \quad (4.11)$$

with $\Delta = 16\sqrt{N/\pi S a} (K_y^3 K_z)^{1/4} e^{-\mathcal{S}_0}$. Taking the limit $\beta \rightarrow \infty$ in Eq. (4.11) we conclude that the ground-state energy of the individual potential wells $\omega_l/2$ is split into two levels separated by Δ provided the total spin NS of the particle is integer. For NS a half odd integer no splitting occurs. Thus for arbitrary spin S the splitting ΔE between the two states of lowest energy is given by

$$\Delta E = |\cos(\pi NS)| \Delta. \quad (4.12)$$

Thus in the uniform limit our theory reproduces the spin parity effect of Ref. 18; moreover, in the limit $K_y \ll K_z$, the tunneling exponent agrees with Refs. 60 and 9 and Δ with Ref. 7.

V. BLOCH WALLS AND SPIN WAVES

In this section we discuss the interaction between a Bloch wall and its surrounding spin waves. We consider here a sample with N_A (or S) sufficiently large such that spin waves are just a small perturbation of the Bloch wall. For a quantitative description of this interaction we use a systematic approach with the ratio of wall velocity to spin wave velocity \dot{X}/c as a small parameter. This is justified since typically $\dot{X} \ll c \sim 10^4$ cm/s. We construct then an *ab initio* theory for the soliton dissipation by integrating out the spin waves. Finally, by deriving the spectral function of the damping kernel we can make contact with the phenomenological Caldeira-Leggett formalism of dissipation.³⁵ A brief account of the following results has been given in Refs. 21 and 24.

We consider elongated samples (cf. Fig. 1) of sufficiently small cross sectional area such that the transverse spin waves^{44,38} around the Bloch wall are frozen out.⁴⁵ This condition typically requires N_A to be less than 10^3 , and thus can easily be reconciled with the above condition that $N_A \gg 1$. Motivated by materials such as YIG which are favorable for MQP we consider the limit of large hard-axis anisotropy. This allows us to build upon the results of the last section and we can treat the interaction between Bloch wall and spin waves within the sine-Gordon model.³³

For notational simplicity we restrict ourselves for the moment to one of the Bloch walls (3.3), $\phi_0(x) = \phi_{Q=1, C=1}(x)$. First we recall that $\phi_0(x-X)$ is, for arbitrary X , a static solution of $\delta \mathcal{S}_{SG} = 0$. We now consider field configurations describing a Bloch wall at a position X surrounded by arbitrary spin waves φ ,

$$\phi(x, \tau) = \phi_0(x-X) + \varphi(x-X, \tau), \quad (5.1)$$

and *elevate* $X(\tau)$ to a dynamical variable. However, Eq. (5.1) contains now a redundant description of a rigid translation of the soliton: A translation is described either by X or by the ‘‘zero-mode’’ (Goldstone mode) $\varphi_0(x, \tau) \propto \phi'_0(x)$.^{61–63,59} To avoid double counting, we thus have to impose the constraint that the spin wave modes be orthogonal to the zero mode

$$\int dx \phi'_0(x) \varphi(x, \tau) = 0, \quad (5.2)$$

for all imaginary times τ . We incorporate this constraint into the path integral by means of the Faddeev-Popov technique^{62,63} which we now briefly sketch. It is based on the identity

$$\int \mathcal{D}X \delta(Q[X]) \det \frac{\delta Q}{\delta X} = 1, \quad (5.3)$$

with the judiciously^{63,64} chosen functional

$$Q[X] = \int dx \phi'_0(x-X) \phi(x, \tau). \quad (5.4)$$

Inserting (5.1) into (5.4) we recognize that the δ function enforces the constraint (5.2) as desired.

For configurations which contain one soliton, we thus can rewrite the transition amplitude (4.3) as follows:

$$\langle \{\Omega_b\} | e^{-\beta \mathcal{H}} | \{\Omega_a\} \rangle = \int \mathcal{D}X \mathcal{D}\phi \delta(Q) \det \left(\frac{\delta Q}{\delta X} \right) e^{-\mathcal{S}_{sc}[\phi]}, \quad (5.5)$$

where the action is given by (4.4). We now perform a systematic expansion up to second order in both spin waves φ and \dot{X}/c . (Note that $\dot{X}/c < 1.5 \times 10^{-2}$ for YIG as discussed in Sec. VII and $\varphi \propto 1/\sqrt{N_A}$ as we shall see below.) After insertion of (5.1) into (5.5) and expansion to second order in the spin waves φ and second order in the Bloch wall velocity \dot{X}/c , the transition amplitude takes the form

$$\langle \{\Omega_b\} | e^{-\beta \mathcal{H}} | \{\Omega_a\} \rangle = \int \mathcal{D}X e^{-S_X[X]} F[X], \quad (5.6)$$

where

$$\mathcal{S}_X = \int d\tau \left\{ -i\alpha \dot{X} + \frac{M}{2} \dot{X}^2 \right\} \quad (5.7)$$

is the action of a free Bloch wall, and where

$$F[X] = \int \mathcal{D}\varphi \delta \left(\int \phi'_0 \varphi \right) \det \left(\frac{\delta Q}{\delta X} \right) e^{-N_A \{ \varphi \cdot [\mathcal{S} + \mathcal{H}] \varphi + \mathcal{I} \cdot \varphi \}} \quad (5.8)$$

describes the interaction between the Bloch wall and the spin waves. Here we have introduced the scalar product $a \cdot b = \int dx d\tau a^* b$ and the integral in the δ function is understood as an integral over x .

We now discuss the various terms that have been introduced in (5.6)–(5.8). The first term in the action (5.7) has the form of a gauge potential

$$\alpha = \pi S N_A / a. \quad (5.9)$$

It originates from the topological term in (4.4) and from the relation $\int dx \partial_\tau \phi_0(x-X) = -\pi \dot{X}$ since each soliton flips the spins by $\pi = \int dx \phi'_0$.

The second term in (5.7) is the kinetic energy of the Bloch wall and the mass is given by

$$M = \frac{E_0}{c^2} = \frac{N_A S^2}{a^2} \sqrt{\frac{K_y}{J}} \frac{1}{K_z}. \quad (5.10)$$

This value coincides with the Döring mass⁴⁷ $M = N_A a^2 / (2\pi\gamma^2\delta)$ with $\gamma = g\mu_B/\hbar$ if the hard-axis anisotropy is of purely demagnetizing origin, $K_z = 2\pi M_0^2 a^2$ with $M_0 = g\mu_B S/a^3$. We thus have given a *microscopic derivation of the Döring wall mass*.

In (5.7) we have dropped a term βE_0 with E_0 the Bloch wall energy (3.5) since the Bloch wall already exists in the sample and is not created thermally. The thermal creation of Bloch wall pairs in the absence of an external field is negligibly small for temperatures in the kelvin range even for samples as small as $50 \text{ \AA} \times 50 \text{ \AA}$. Only at higher temperatures and in the presence of external fields does thermal creation of Bloch wall pairs become appreciable.⁶⁵

The functional F (5.8) describes the coupling between spin waves and the Bloch wall. The operator⁴³

$$\mathcal{G} = -J\partial_x^2 - \kappa\partial_\tau^2 + K_y \left[1 - 2 \operatorname{sech}^2\left(\frac{x}{\delta}\right) \right] \quad (5.11)$$

with $\kappa = J/c^2$ describes the spin wave spectrum around a static Bloch wall. The remaining operators are responsible for the dynamic coupling between spin waves and domain wall,

$$\mathcal{H} = 2\kappa\dot{X}\partial_x\partial_\tau - \kappa\dot{X}^2\partial_x^2, \quad \mathcal{J} = -2\kappa\dot{X}^2\phi_0''. \quad (5.12)$$

Due to the constraint (5.2) the exponential in F , Eq. (5.8), does not contain a term linear in the velocity \dot{X} and in the spin waves φ . It has been pointed out^{30,31} that this is an important difference from the standard Caldeira-Leggett model.³⁵ However, despite this nonlinear coupling we shall see shortly that at low temperatures the dissipation due to spin waves can — if this should be desirable — perfectly well be modeled by a Caldeira-Leggett approach (such cases have actually been discussed in Appendix I of Ref. 35), although the precise form of the relevant spectral function can only be obtained from a microscopic calculation as presented here.

After the evaluation of (5.5) which is sketched in Appendix B and collecting Eqs. (5.7), (B4), (B5), and (B17) we can express the transition amplitude (5.6) as

$$\langle \{\mathbf{\Omega}_b\} | e^{-\beta\mathcal{H}} | \{\mathbf{\Omega}_a\} \rangle = \int \mathcal{D}X e^{-\mathcal{S}_{\text{eff}}[X]}, \quad (5.13)$$

with the effective action for the soliton position

$$\begin{aligned} \mathcal{S}_{\text{eff}}[X] = & \int_0^\beta d\tau \left\{ -i\alpha\dot{X} + \frac{M_{\text{eff}}}{2}\dot{X}^2 \right\} \\ & + \frac{1}{2} \int_0^\beta d\tau \int_0^\tau d\sigma K(\tau-\sigma) [X(\tau) - X(\sigma)]^2. \end{aligned} \quad (5.14)$$

The damping kernel has been evaluated for arbitrary temperatures in Appendix B. Here we restrict ourselves to low temperatures, $\beta \rightarrow \infty$, where the damping kernel (B19) takes the form

$$K(\tau) = -2 \sum_k k^2 \omega_k^2 e^{-2\omega_k|\tau|}. \quad (5.15)$$

This can also be cast into standard Caldeira-Leggett notation,^{35,36}

$$K(\tau) = \frac{1}{\pi} \int_0^\infty d\omega J(\omega) D_\omega(\tau). \quad (5.16)$$

Here $D_\omega(\tau) = e^{-\omega|\tau|}$ is the $T \rightarrow 0$ limit of (B18) and the spectral function is given by⁶⁶

$$J(\omega) = \frac{\omega}{\omega_0 \delta^2} \Theta(\omega - \omega_0) \sqrt{\omega^2 - \omega_0^2}, \quad (5.17)$$

which vanishes for $\omega < \omega_0 \equiv 2c/\delta = (4a/S)\sqrt{K_y K_z}$, the anisotropy gap of the spin waves. (For material values as in YIG, this gap corresponds to a temperature of $T_g = 0.2 \text{ K}$. Other materials have in general larger anisotropies and thus higher T_g .) In deriving (5.17) from (5.15) we have used the renormalization (B10). It is only after this renormalization that the memory kernel K becomes positive definite (as is needed for convergence).

If now the dynamics of X is slow compared to the time variation of the damping kernel, i.e., if the instanton frequency ω_I (to be evaluated below) is much smaller than $\omega_0 = 2c/\delta$, and if the temperature is small such that $\beta \gg \omega_I^{-1}$, then we may expand $X(\tau) - X(\sigma) \approx (\tau - \sigma)\dot{X}(\sigma)$, and the damping kernel reduces to a pure mass renormalization. Note that this mass renormalization is an $O((N_A)^0)$ correction of the wall mass $M \propto N_A$. Since all these conditions will be satisfied for the tunneling situations considered below, we see that we end up with a deceptively simple effective description of the Bloch wall dynamics, given by the first two terms in (5.14).

VI. INTERFERENCE EFFECTS DUE TO THE BERRY PHASE

In the last section we derived an effective action for the dynamics of the Bloch wall position. We showed that damping due to spin waves leads to a gap in the spectral function and thus leads to a mere renormalization of the wall mass at low temperatures. More importantly, we have identified a topological term in the action which has its origin in the Berry phase term (2.4) of the original spin action.

Here we shall generalize these considerations to solitons ϕ_{QC} of arbitrary chirality C and charge Q which are all energetically degenerate. We show that the interference between states of different chirality gives rise to remarkable effects such as the halving of the Brillouin zone and the alternation of chirality in reciprocal space for half-integral spin.

These effects originate in the fact that for arbitrary solitons, the topological term (2.4)

$$i\frac{\alpha}{\pi} \int dx \dot{\phi}_{QC}(x-X) = -i\alpha C \dot{X} \quad (6.1)$$

depends on the soliton chirality C (but not on its charge Q) ($\alpha = \pi S N_A / a$). This chirality dependence can intuitively be understood as follows. As the soliton sweeps across a given

spin, the spin is rotated by an angle $\pm \pi$ (after the wall is sufficiently far away), the rotation sense being uniquely determined by the chirality and the direction of motion of the Bloch wall.

At low temperatures and for solitons of arbitrary chirality the effective action (5.14) of a soliton in an external potential $V(X)$ thus takes the form

$$\mathcal{A}[X, C] = \int d\tau \left\{ -i\alpha C \dot{X} + \frac{M}{2} \dot{X}^2 + V(X) \right\}. \quad (6.2)$$

Here we have used the mass (5.10) rather than the dressed mass M_{eff} since the mass renormalizations at low temperatures are small $O((N_A)^0)$ and the value (5.10) thus represents a good approximation for the experimentally observed wall mass. In addition we have introduced a periodic potential $V(X)$ of period d , and we make the natural assumption that d is some integer multiple of the lattice constant a . For definiteness we assume

$$V(X) = V_0 \left[1 - \cos\left(\frac{2\pi X}{d}\right) \right], \quad (6.3)$$

which has amplitude $2V_0$.⁶⁷ Such a potential can have its origin^{24,21} in the discrete nature of the crystal lattice itself, or for Bloch walls it can arise from a magnetic superlattice of layers with different anisotropies.

The action (6.2) corresponds to the Hamiltonian

$$\mathcal{H} = \frac{1}{2M} (p - \alpha\sigma_z)^2 + V(X), \quad (6.4)$$

where $p = -i\partial/\partial X$ is the Bloch wall momentum and σ_z is the Pauli matrix of the ‘‘pseudospin’’ characterizing the chirality $C = \pm$ of the Bloch wall. Obviously, this Hamiltonian conserves the chirality. For mathematical convenience, we choose periodic boundary conditions in the following. However, all our results are finite in the thermodynamic limit and none of our conclusions depend on this choice of boundary conditions.⁶⁸

From both (6.2) and (6.4) it is evident that the topological phase plays the role of a gauge potential whose effect on the wall dynamics will be discussed next. We note that such spin-dependent gauge potentials are not uncommon in problems involving Berry phases.⁶⁹

A. An illustrative example

Before giving a rigorous discussion of the dispersion relation, we give an argument to illustrate the interplay between the topological phase and soliton propagation.

Consider the transition amplitude for the propagation of the Bloch wall between nearest neighbors, which is given by

$$\begin{aligned} \langle 0 | e^{-\beta \mathcal{H}} | d \rangle &= \sum_C \int_0^d \mathcal{D}X e^{i\alpha C \int d\tau \dot{X}} e^{-\mathcal{S}_0} \\ &= 2 \cos(\alpha d) \int_0^d \mathcal{D}X e^{-\mathcal{S}_0}, \end{aligned} \quad (6.5)$$

where $\mathcal{S}_0[X] = \int d\tau \{ (M/2) \dot{X}^2 + V(X) \}$. For half-integer $\sigma \equiv N_A S d/a$, we thus arrive at a most important conclusion: *Nearest-neighbor hopping of the soliton is suppressed if both*

chiralities contribute equally to the transition amplitude. However, if the soliton is in a state of *definite chirality*, only one path contributes to the transition amplitude (6.5) and *nearest-neighbor hopping is allowed.* No such interference occurs for integer σ . Note that this interference effect is entirely due to the topological term in (6.2) which in turn is a consequence of the topological term in the sine-Gordon action (4.4).

We now investigate how this interference affects the dispersion of solitons and in this way can become observable.

B. Dispersion in the nearly free limit

In this section we discuss the dynamics of a soliton in an arbitrarily weak periodic potential $V(X)$. The Hamiltonian is given by (6.4) with $V_0 \rightarrow 0$. Despite being simple this case already captures most of the characteristic features of the tight-binding limit which will be discussed below. For simplicity we assume that the period of the potential is given by $d = a$.

Using periodic boundary conditions, the eigenstates of (6.4) are simply plane waves e^{ikX} , with $k = 2\pi n/L$, $L = Nd$, and the spectrum consists of two parabolas (corresponding to the two soliton chiralities)

$$E(k, C = \pm 1) = \frac{1}{2M} (km \mp \alpha)^2, \quad (6.6)$$

periodically extended by the reciprocal lattice vector $G = 2\pi/a$. [Note that the requirement of gauge invariance alone produces such a periodic extension even in the complete absence of a periodic potential. The gauges (A3) lead to Hamiltonians (6.4) with $\alpha \rightarrow (2n+1)\alpha$ with $n = 0, \pm 1, \dots$. The gauge invariant dispersion is therefore the periodic extension of (6.6) by a vector 2α .]

The Berry phase thus leads to remarkable spin parity effects in the dispersion: For half-odd-integer spin $N_A S$, we have $\alpha = G/4 \pmod{G}$ and the parabolas are separated by half the reciprocal lattice vector, $G/2$. Thus the Brillouin zone is halved and two subsequent parabolas belong to opposite chiralities as illustrated in Fig. 3. The observability of this is discussed in Sec. VI D.

For integer spin, however, the dispersion is analogous to that of a free particle of mass M and the Berry phase is inoperative since it merely shifts the dispersion by a reciprocal lattice vector.

Note that since $\alpha \propto 1/a$ is independent of the sample length, the result is unchanged if we pass to the thermodynamic limit. Therefore (6.6) is independent of the boundary conditions.⁷⁰

C. Tight-binding limit

We now turn to a discussion of the system in the tight-binding limit where $V(X)$ is no longer small. In the absence of tunneling there exists a large number of degenerate ground states corresponding to the soliton trapped at one particular pinning site. If the pinning potential is not too large, the soliton can tunnel between the sites, and these ground states split into the (lowest) band $E(k, C)$ with

$$\mathcal{H} |k, C\rangle = E(k, C) |k, C\rangle. \quad (6.7)$$

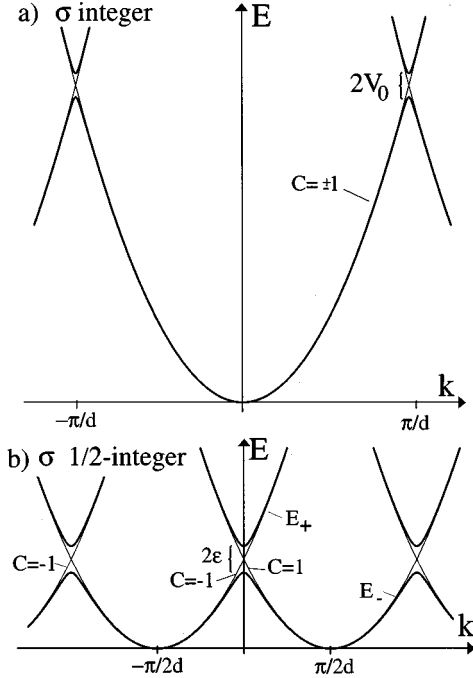


FIG. 3. Dispersion of a soliton in a weak periodic potential. (a) For $\sigma = N_A S d / a$ integer the dispersion resembles that of a Bloch electron and the gaps at $\pm \pi / d$ are due to the periodic pinning potential (6.3). (b) For σ half-odd integer the Brillouin zone is halved and two subsequent band minima have opposite chirality. Band gaps 2ϵ arise due to tunneling between the chiralities as described by (6.22); E_+ and E_- are the dispersions as given by (6.23).

Since \mathcal{H} in (6.4) is invariant under translations by the potential period d and conserves the chirality pseudospin, the eigenstates are products of Bloch states and chirality eigenstates $|k, C\rangle = |k\rangle \otimes |C\rangle$ where $\mathcal{T}|k\rangle = e^{ikd}|k\rangle$ and $\sigma_z|C\rangle = C|C\rangle$ with $k = 2\pi n / Nd$, $n = 0, 1, \dots, N-1$, and $L = Nd$. \mathcal{T} is the translation operator $\langle X | \mathcal{T} = \langle X + d |$.

For the evaluation of the band structure in the tight-binding limit we now develop a formalism which allows us to keep careful track of the topological phases within the instanton approach. To this end we start from the modified partition function⁷¹

$$\mathcal{Z}_l = \text{tr}\{\mathcal{T}^l e^{-\beta \mathcal{H}}\}, \quad (6.8)$$

where $\text{tr}\{\dots\} = \sum_{k,C} \langle k, C | \dots | k, C \rangle$. We use (6.8) rather than the usual partition function $\mathcal{Z} = \text{tr}\{e^{-\beta \mathcal{H}}\}$ for the following reason. As we have seen in the previous section, the Berry phase gives rise to a shift of the dispersion with respect to k . However, the partition function \mathcal{Z} is insensitive to such shifts (at least if there is no perturbation which mixes the chirality states) and thus represents an insufficient tool for the evaluation of the band structure.

From (6.8) we can easily extract the dispersion by taking the Fourier transform

$$\sum_{l=0}^{N-1} e^{-ikld} \mathcal{Z}_l = N \sum_{C=\pm} e^{-\beta E(k,C)}, \quad (6.9)$$

where we used (6.7) and the definition of \mathcal{T} . In addition, we have restricted ourselves to the lowest band since we are interested in the low-temperature limit. Note also that the LHS of (6.9) does not contain higher-winding-number contributions since we are not interested in finite size effects arising from the sample topology. We now evaluate \mathcal{Z}_l and get in a first step

$$\begin{aligned} \mathcal{Z}_l &= \sum_C \int_0^L dX \langle X + ld, C | e^{-\beta \mathcal{H}} | X, C \rangle \\ &= \sum_{C,k} \sum_{m=0}^{N-1} \int_{md-d/2}^{md+d/2} dX |\langle X, C | k \rangle|^2 e^{-\beta E(k,C) + ikld}, \end{aligned} \quad (6.10)$$

where we used periodic boundary conditions and inserted a complete set of Bloch states. Next, in the tight-binding limit the main contributions to the integral are coming from the vicinity of the potential minima, $X \approx md$, and the Bloch functions can be replaced by their harmonic approximations, i.e., $|\langle k | md \rangle|^2 \approx |\psi_h(0)|^2 / N = a_0 / N$. Here, ψ_h is the ground state in the harmonic approximation of the potential well and $a_0 = \sqrt{M\omega/\pi}$ its normalization (squared). Thus we find

$$\mathcal{Z}_l \approx \frac{1}{a_0} \sum_C \sum_{m=0}^{N-1} \langle md + ld, C | e^{-\beta \mathcal{H}} | md, C \rangle. \quad (6.11)$$

Using a path integral representation for (6.11) and employing the periodicity of \mathcal{H} we obtain with (6.9)

$$\sum_C e^{-\beta E(k,C)} = \frac{1}{a_0} \sum_{C,l=0}^{N-1} e^{-ikld} \int_{X(0)=0}^{X(\beta)=ld} \mathcal{D}X e^{-\mathcal{S}[X,C]}, \quad (6.12)$$

with $\mathcal{S}[X,C]$ as in (6.2). The path integral on the RHS of (6.12) is dominated by instantons between the potential minima. These instantons obey the Euler-Lagrange equation $\delta \mathcal{S} / \delta X = -M\ddot{X} + V'(X) = 0$. For instance, a transition from $X=0$ to $X=d$ ($X=-d$) is mediated by the (anti-) instanton

$$X^\pm = \pm \frac{2d}{\pi} \arctan e^{\omega(\tau - \tau_0)}, \quad (6.13)$$

centered at the arbitrary imaginary time τ_0 . The instanton frequency $\omega = (2\pi/d)\sqrt{V_0/M}$ equals the harmonic oscillation frequency in the potential well. The instanton action is given by

$$\mathcal{S}_\pm = \mathcal{S}[X^\pm, C] = \mathcal{S}_0 \mp iadC, \quad (6.14)$$

where $\mathcal{S}_0 = (4/\pi)d\sqrt{MV_0} = 8(V_0/\omega)$. The unusual second term in (6.14) is purely imaginary and is a direct consequence of the gauge potential in (5.14) or (6.4) and distinguishes between instantons and anti-instantons. Note that this term does not break time reversal invariance as the partition function contains contributions of both chirality states $C = \pm 1$.

The path integral in (6.12) can be expressed as the sum over all distinct sequences of n_+ instantons and $n_- = n_+ - l$ anti-instantons which connect the initial state $X=0$ with the final state $X(\beta) = ld$. Within this ‘‘dilute instanton gas approximation’’⁵⁹ we obtain

$$\begin{aligned}
& \int_{X(0)=0}^{X(\beta)=ld} \mathcal{D}X e^{-\mathcal{A}[X,C]} \\
&= a_0 e^{-\beta\omega/2} \sum_{n_+, n_- = 0}^{\infty} \delta_{n_+, n_- + l} \\
& \times \frac{(JK\beta e^{-\mathcal{J}_+})^{n_+}}{n_+!} \frac{(JK\beta e^{-\mathcal{J}_-})^{n_-}}{n_-!}, \quad (6.15)
\end{aligned}$$

where $J = \sqrt{\mathcal{J}_0/2\pi M}$ and $K = 2\omega\sqrt{M}$ arise from the integration over the zero modes and the Gaussian fluctuations around an instanton, respectively. Inserting (6.15) into (6.12), using (6.14), and performing the sums, we obtain

$$\sum_C e^{-\beta E(k,C)} = \sum_C e^{-\beta[\omega/2 + \epsilon(k,C)]}, \quad (6.16)$$

where

$$\epsilon(k,C) = -2JK e^{-\mathcal{J}_0} \cos[(k + \alpha C)d]. \quad (6.17)$$

The ground state as a function of k is given by

$$E(k) = -\lim_{\beta \rightarrow \infty} \frac{1}{\beta} \ln \sum_C e^{-\beta E(k,C)}. \quad (6.18)$$

Similarly to the nearly free limit discussed in the previous subsection, this dispersion is fundamentally different for $\sigma \equiv \alpha d/\pi = N_A S d/a$ integer or half-odd integer.²¹

Inserting (6.16) into (6.18) we obtain for integer σ the following dispersion:

$$E(k) = -\frac{\Delta}{2} \cos(kd), \quad (6.19)$$

which is of standard tight-binding type. In (6.19) we dropped the constant $\omega/2$. The bandwidth is given by

$$\Delta = 8\omega \sqrt{\frac{\mathcal{J}_0}{2\pi}} e^{-\mathcal{J}_0}. \quad (6.20)$$

In contrast, for σ half-integer we obtain

$$E(k) = -\frac{\Delta}{2} |\sin(kd)|. \quad (6.21)$$

In (6.19) and (6.21) we have suppressed sign changes which correspond to a global shift of k by π/d . Such a global sign cannot be measured since the absolute value of k is experimentally not detectable.

The dispersion (6.21) now has cusps and *the bandwidth and the Brillouin zone are halved*,⁷² as shown in Fig. 3. Moreover, we draw from (6.16) and (6.18) the important conclusion that *states whose wave vectors differ by π have opposite chirality*, cf. Fig. 4.

Note that this period halving in reciprocal space is a consequence of the fact that $\mathcal{Z}_l = \sum_C \int_0^ld \mathcal{D}X e^{-\mathcal{A}[X,C]} = 0$ for l odd [cf. (6.5)]. However, one must not conclude from this fact that nearest-neighbor hopping is always suppressed: At fixed $k \neq 0, \pm \pi/d$, the ground-state condition (6.18) selects a branch of the dispersion with *definite* chirality, a dispersion that results from nearest-neighbor hopping. Only at the cusps in (6.21) is hopping suppressed.

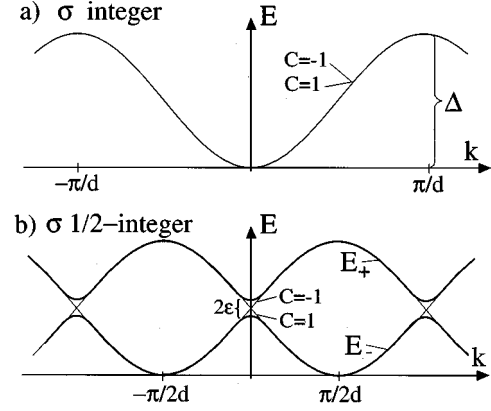


FIG. 4. Soliton dispersion in the tight-binding limit. (a) For $\sigma = N_A S d/a$ integer a standard tight-binding dispersion results. (b) For σ half-odd integer, the Brillouin zone (and bandwidth) is halved and two subsequent band minima belong to opposite chiralities. A gap 2ϵ develops if the two chiralities of the soliton are connected by tunneling.

This band halving can also be understood in a more intuitive way: For half-integer σ , a soliton acquires a Berry phase iC for forward ($-iC$ for backward) hopping. In the ground state this phase gets compensated by the Bloch phase, thus creating two band minima at $kd = \pm \pi/2$ which have opposite chirality.

Finally, we give a more explicit formal argument for the chirality correlation. We find the explicit form of the eigenvalue $E(k,C)$ by repeating the steps leading to Eq. (6.16), but instead of \mathcal{Z}_l we use $\mathcal{Z}_l^C = \text{tr}\{|C\rangle\langle C| \mathcal{A} e^{-\beta \mathcal{H}}\}$, which projects onto a state of definite chirality C . Thus we find that $E(k,C)$ is given by $\epsilon(k,C)$ in Eq. (6.17). By comparing the ground-state energy (6.21) with $E(k,C)$ we see that k intervals with positive (negative) $\sin kd$ belong to negative (positive) chirality C . This result is derived in the north-pole parametrization. If, instead, we use the south-pole parametrization, then the gauge potential in (6.2) changes sign and again we find that the chirality alternates, but now with the opposite assignment between chirality and a given k interval. The physical consequence—alternating chirality with changing k —is the same in the two gauges, since, again, the absolute k value cannot be observed.

D. Discussion and analogies to other physical systems

In the last two sections we have seen that the dispersion is strongly affected by the parity of $\sigma = N_A S d/a$. For σ integer, the dispersion equals that of a particle in a periodic potential while for σ half-integer a halving of the Brillouin zone occurs with alternating chiralities. In the latter case the dispersion consists of mutually intersecting parabolas or tight-binding bands. How can we observe such a dispersion?

Let us for definiteness focus on the nearly free limit with a dispersion as shown in Fig. 3. Suppose the chirality has been measured to be $C = 1$ and the system is in its ground state, i.e., in the minimum of a $C = 1$ parabola. If we now drive the system out of its energy minimum, e.g., by applying an external field along the easy axis (see below), the Bloch wall will follow the $C = 1$ parabola. The Bloch wall

will remain on this parabola even beyond the crossing point, *provided* that the chirality C is a conserved quantity. In this sense, the two parabolas for $C=1$ and $C=-1$ behave like two different “sheets” of the energy which are completely disconnected, and their intersection has no observable consequences if there is no mixing, i.e., tunneling, between the chiralities of the Bloch wall.

Nevertheless, the dispersion of Fig. 3 (thin line) is a precursor of a striking physical effect: As soon as there is tunneling between the chiralities, the different “sheets” get connected and for half-integer spins a gap develops at the crossing points of parabolas belonging to $C=\pm 1$. At the same time the halving of the Brillouin zone becomes observable. Formally this can be described as follows. In the presence of tunneling between the two wall chiralities (see Sec. VII) the Hamiltonian (6.4) acquires an additional term $\epsilon\sigma_x$,

$$\mathcal{H} = \frac{1}{2M}(p - \alpha\sigma_z)^2 + V(X) + \epsilon\sigma_x, \quad (6.22)$$

such that the chirality C (i.e., σ_z) is no longer a conserved quantity. We are interested in the limit of small chirality tunneling and therefore ϵ will be much smaller than the bandwidth Δ (estimates for ϵ will be given in Sec. VII). For σ half odd integer, the degeneracy at the points $k_n = n\pi/a$ is lifted and the dispersion splits into two bands which for $|k - k_n| \ll \pi/a$ are given by

$$E_{\pm}(k) = \frac{1}{2M}[(k - k_n)^2 + \alpha^2 \pm \sqrt{4\alpha^2(k - k_n)^2 + \tilde{\epsilon}^2}], \quad (6.23)$$

with $\tilde{\epsilon} = 2M\epsilon$ and where, for simplicity, we have stated the result in the nearly free limit. In this and the tight-binding limit the two bands are separated by a gap 2ϵ at $k = k_n$, as shown in Figs. 3 and 4.

Solving for the corresponding eigenstates we recognize that the chirality continuously switches from $C = \pm 1$ to $C = \mp 1$ as we pass from one band minimum to an adjacent one.

We thus have established that the spectrum given in (6.6) and (6.21) is reached in the limit $\epsilon \rightarrow 0$. Note that the experimental observation of the gap depends on the probability of Zener interband transitions and thus on the time scale at which the band structure is probed. In the nearly free limit, the Zener probability⁷³ can be expressed as^{24,21} $P \propto \exp\{-(\pi/2)(\epsilon^2 T/\hbar E_0)\}$, where $T = 2\pi/\omega_B$ is the time to cross the Brillouin zone, with $\omega_B = Fd/\hbar$ being the Bloch frequency and $F = 2g\mu_B S N_A H/a$ the driving force due to an external field H (along, say, the easy axis, see Sec. VIII). $E_0 = (\hbar^2/2M)(\pi/d)^2$ is the kinetic energy at the zone boundary. Thus, to optimize observability we must have $A = (\pi/2)(\epsilon^2 T/\hbar E_0) \gg 1$, which is easy to achieve since typically $T \sim 10^{-7}$ s, giving $A \sim 100$ for YIG, if we choose $H \sim 10^{-3}$ Oe, $d = a$, and $\epsilon \sim E_0/10 \sim 10$ mK k_B (see Sec. VII). The alternation of chirality could then be observed, for instance, by (optical) dichroism techniques which would be sensitive to the rotation sense of the magnetization within the Bloch wall.

We emphasize that these results are gauge independent. If, instead, we had started from the south-pole parametrization

of the coherent states, we would have obtained the same dispersion (6.6), (6.19), and (6.21), except for a global shift $k \rightarrow k + 2\alpha$ which is unobservable.

A dispersion consisting of disjoint parabolas dictated by gauge invariance and the formation of gaps due to tunneling is quite a common phenomenon in condensed matter physics. Persistent currents in isolated metal rings,⁷⁴ the Josephson effect,⁷⁵ and the tunneling of quasiparticles between edge states in the fractional quantum Hall regime⁷⁶ might serve as familiar examples.

For further illustration let us briefly discuss some relations between our spin effect and, say, persistent currents. First, in the spin system the dispersion remains unaltered in the thermodynamic limit, whereas persistent currents are a finite size effect, resulting from the discreteness of the energy levels. In addition, we consider a simply connected sample topology while a persistent current relies on the ring geometry of the sample. In the spin system it is the S^1 topology of spin space restricted to the easy plane, not the topology of the sample, which is responsible for the interference effect.

An electron of mass m confined to a ring of radius ρ which is threaded by the electromagnetic flux Φ is described by the Hamiltonian

$$\mathcal{H} = \frac{\hbar^2}{2m\rho^2}(-i\partial_\theta - \Phi)^2, \quad (6.24)$$

where Φ is measured in units of the flux quantum $\Phi_0 = hc/e$, and θ is the azimuthal angle. The eigenfunctions are $e^{in\theta}$ with eigenvalues $E_n = (\hbar^2/2m\rho^2)(n - \Phi)^2$, where $n = 0, \pm 1, \dots$. The ground-state energy E_G as a function of flux is the envelope of the set of energy parabolas separated by Φ_0 .⁷⁷ Thus the persistent current $j = -(e/\hbar)\partial E_G/\partial\Phi$ is a sawtooth curve with discontinuities at $|\Phi| = n/2$ where the parabolas intersect. Suppose now that $\Phi = 0$ and that the system is in its ground state with $n = 0$. If the flux is increased adiabatically, the system will stay on the $n = 0$ parabola even for $\Phi > 1/2$ since the angular momentum is a conserved quantity. Thus the electron will not see the other parabolas and the spectrum consists of disconnected “sheets” of parabolas. This behavior is analogous to that for the soliton dispersion (6.6) for half-integer spin.

However, if angular momentum is no longer conserved, e.g., due to the presence of a scattering potential, the parabolas will be connected and a gap develops at their crossing points. The scattering potential thus plays a role similar to the $\epsilon\sigma_x$ term in (6.22) caused by tunneling between the chiralities.

The mere existence of interference effects in a metal ring can also be derived from the following argument. Assume that $\Phi = 1/2$ and let us imagine having prepared two wave packets of opposite angular momentum, but otherwise identical. If we let these wave packets dynamically evolve until they have traveled half the circumference, one clockwise and the other anticlockwise, they will have picked up Aharonov-Bohm phases of opposite sign such that (for $\Phi = 1/2$) destructive interference occurs, leading to a vanishing transition amplitude between initial and final states. This behavior is similar to the spin case described in (6.5), where the clockwise and anticlockwise traveling wave packets correspond to

the two chirality states of the soliton (note again that the real space topology of the ferromagnet is irrelevant).

VII. EXPERIMENTAL IMPLICATIONS

In this section we give numerical estimates for the effects discussed in the previous sections. For definiteness we concentrate on material parameters for YIG. Exchange⁷⁸ and anisotropy⁷⁹ are given by $J=1.65\times 10^{-21}$ erg/cm and $K_y=9.61\times 10^{-11}$ erg/cm, where a cell with lattice constant $a=6.2$ Å contains one $S=5/2$ spin implying a saturation magnetization⁷⁹ of $M_0=194$ Oe (i.e., $K_z=2\pi M_0^2 a^2=9.1\times 10^{-10}$ erg/cm), wall width $\delta=\sqrt{J/K_y}=414$ Å, and spin wave velocity, Eq. (4.5), $c=6\times 10^4$ cm/s. The pinning potential strength can be related to an experimentally observed coercivity by adding²⁹ a Zeeman term $-2\mathcal{A}M_0H_{\text{ext}}X$ to the pinning potential $V(X)$, with $\mathcal{A}=N_A a^2$ the cross sectional area of the sample. Defining the coercivity H_c as the field at which the barrier height vanishes, we obtain $V_0/\mathcal{A}=H_c M_0 d/\pi$. Note that the coercivity is proportional to the slope V_0/d of the potential. Looking at the WKB exponent (6.14), $\mathcal{S}_0=(4/\pi)d\sqrt{MV_0}$, we see that a low coercivity does not necessarily imply a high tunneling probability. The crucial condition is a small potential width d .

We now assume a coercivity⁸⁰ of $H_c=2$ Oe and $d=3a$. Note that the wall extends over 22 pinning sites. The instanton frequency then becomes $\omega=(2\pi/d)\sqrt{V_0/M}=1.4\times 10^{10}$ s⁻¹, and $|\dot{X}/c|=\omega d/\pi c\leq 1.5\times 10^{-2}$. For a sample with cross sectional area $\mathcal{A}=10^4$ Å² we have $N_A=260$, and the wall contains $N_A\delta/a=2\times 10^4$ spins. The pinning potential height takes the value $2V_0=330$ mK k_B , and the bandwidth (6.20) is $\Delta/\hbar\approx 10^6$ s⁻¹, which is of the order of the measured resonance frequency in Ref. 15. The Döring mass, Eq. (5.10), corresponding to this cross sectional area \mathcal{A} takes the value $M=1.24\times 10^{-22}$ g $(=1.36\times 10^5)m_e$, where m_e is the electron mass. The crossover temperature between quantum tunneling and thermally activated behavior is $T_c=2V_0\hbar/\mathcal{S}_0k_B=\hbar\omega/4k_B\approx 28$ mK, since $\hbar\omega/k_B=110$ mK for $d=3a$. Note that the bandwidth is extremely sensitive to the details of the pinning potential. For instance, if $d=a$ (lattice pinning) but all other parameters are chosen as above, we obtain $\omega=2.5\times 10^{10}$ s⁻¹ (corresponding to 190 mK), and $\Delta/\hbar\approx 1.2\times 10^{10}$ s⁻¹ (since $\mathcal{S}_0/\hbar=2.3$), or $\Delta\approx 0.8$ times the pinning potential height $2V_0=110$ mK k_B , while $T_c\approx 48$ mK.

We emphasize that these numbers are rather material dependent. For instance, in an orthoferrite, a canted antiferromagnet, the effective wall mass is by a factor 10^3 smaller⁴⁷ than the value obtained from the Döring wall mass (5.10). Thus tunneling could also occur at much larger potential heights and higher crossover temperatures.

Next, we briefly address the issue of impurities;²¹ a more detailed account will be given elsewhere.³⁴ The analysis so far was based on the fact that the magnetic field is constant throughout the sample. A single impurity (or similarly an inhomogeneous field) can be incorporated into the energy (2.5) by adding a term $\kappa a\delta(x-x_0)\sin^2\phi$ where κ is of the order of the anisotropy constant K_y . Although the impurity is pointlike, it leads to an *extended* potential

$U(X)=-\kappa a\text{sech}^2[(X-x_0)/\delta]$ of width δ for the wall center. Thus even when κa is of the order of the strength $2V_0$ of the periodic potential, the impurity potential only leads to a small variation $(d/\delta)\kappa a$ between pinning sites separated by $d\ll\delta$. This holds also for a random impurity distribution even in the unrealistic case (for YIG) of high disorder with one impurity per transverse layer. Under the action of an external field H_y along the easy axis, which can be much smaller than the coercivity H_c , all wells created by the impurities can be rendered unstable such that they no longer trap the wall. Localization of the wall is then determined by quantum interference effects only which we can characterize by the Anderson localization length. This length, however, is sufficiently large and explicitly given by $aN_A^2(\Delta/2V_0)^2\approx(5\times 10^4)a$.³⁴

We note that tunneling in periodic pinning potentials allows much higher crossover temperatures than tunneling out of a single isolated (metastable) potential. Indeed, in the presence of an external field along the easy axis the total energy is $U(X)=-V_0\text{sech}^2X/\delta-2\mathcal{A}M_0H_{\text{ext}}X$ where $V_0=(3\sqrt{3}/2)\delta\mathcal{A}M_0H_c$. The crossover temperature and the WKB exponent are then given by $T_c=2^{3/4}(5/18)(g\mu_B/k_B)\sqrt{\pi H_c M_0}\bar{\epsilon}^{1/4}$ and $\mathcal{S}_0=2^{3/4}(6/5)\hbar N_s\times\sqrt{H_c/\pi M_0}\bar{\epsilon}^{5/4}$ where $\bar{\epsilon}=1-H_{\text{ext}}/H_c$. For example, for a YIG sample of 50 Å \times 200 Å with $H_c=10$ Oe, this leads to crossover temperatures in the millikelvin range $0.5<T_c<1.4$ mK while the WKB exponent changes in the interval $0.2<\mathcal{S}_0/\hbar<31.1$.

We now turn to a discussion of *quantum tunneling between the two chirality states of a soliton*. We shall obtain explicit estimates for the level splitting ϵ introduced in Eq. (6.22). In addition, we shall see that chirality tunneling provides a scenario for mesoscopic quantum coherence with one important advantage that both barrier height and bias of the double well can be tuned independently by external fields.

Chirality tunneling involves rotation of the spins out of the easy plane and thus cannot be described within the XY approximation which we have used so far. To treat this case we must go back to the full action (2.3) and deal with both polar angles ϕ and θ . The generalization of the wall dynamics to this situation, in particular, the reduction to the collective coordinate and the dissipation due to spin waves, is necessarily more involved but still feasible.³⁴ However, since this generalization is somewhat outside the scope of the present work we shall only quote the essential results here and give the details in a forthcoming paper.³⁴ For definiteness we concentrate now on ferromagnets where the easy-axis anisotropy exceeds the one along the hard axis, i.e., $K_y\gg K_z$; typical examples are bubble materials.⁴⁷ To take advantage of the resulting approximate symmetry around the z axis, we represent the magnetization field as $\mathbf{\Omega}=(\sin\theta\sin\phi, \cos\theta, \sin\theta\cos\phi)$.⁴⁷ The Bloch wall is then described by a rotation of the spins in the xy plane about the angle θ , and the chirality switching by a rotation in the xz plane about the angle $\phi=\pm\pi$. In addition, we allow for an external magnetic field H_z along the hard axis z with which one can tune the barrier height that separates the two wall chiralities.

We now integrate out the θ fluctuations around the Bloch wall and restrict ourselves to uniform rotations in ϕ (which is valid⁴⁷ if the wall width δ is less than $\sqrt{J/K_z}$). After a

careful treatment of the zero mode, we obtain an effective Lagrangian in $\phi(\tau)$,

$$\mathcal{L}_c = \frac{M_c}{2} \dot{\phi}^2 + V(\phi), \quad (7.1)$$

$$V = \kappa \cos^2 \phi + \eta \cos \phi + \eta^2/4\kappa, \quad (7.2)$$

where $M_c = N_A S^2 \pi^2 \delta / 8a^2 K_y$ is the effective mass associated with the chirality dynamics, and the parameters $\kappa = 2\delta N_A K_z$ and $\eta = g\mu_B S N_A \pi \delta H_z / a$ characterize the barrier potential V . Defining the anisotropy field by $H_a = 4aK_z / g\mu_B S \pi$ and noting that the chirality tunnels between the potential minima defined by $\cos\phi_{\min} = -H_z/H_a \equiv \nu - 1$, we obtain for the level splitting ϵ

$$\epsilon = 4\gamma\omega_c \sqrt{\mathcal{S}_c/2\pi} e^{-S_c}, \quad (7.3)$$

where γ is a numerical constant of order 1. The instanton action \mathcal{S}_c and frequency ω_c are given by

$$\mathcal{S}_c = 2\pi S(N_A \delta/a) \sqrt{\frac{K_z}{K_y}} \nu^{3/2}, \quad (7.4)$$

$$\omega_c = \frac{8a}{\pi} \sqrt{K_y K_z} \nu^{1/2}. \quad (7.5)$$

The crossover temperature becomes $T_c = \omega_c / 8k_B$. Note the characteristic power dependence on the external control parameter $\nu = 1 - H_z/H_a$ with which the chirality splitting ϵ can be changed over a large range. In the next section we shall also see how a field H_x can be used to offset unwanted bias between the potential minima.

We illustrate these results with some typical numbers. Choosing $N_A \delta/a \sim 10^4$, $K_y/K_z \sim 10$, $\nu \sim 10^{-3}$, $aK_z \sim 1$ K k_B , and $S = 5/2$, we find for the chirality splitting $\epsilon \approx 5$ mK k_B , while the crossover temperature is $T_c \approx 13$ mK. The values for the bandwidth Δ are roughly the same as before. This shows that the splitting ϵ can be made quite large (on the scale of Δ) just by tuning the external field along the hard axis, while the crossover temperature is still reasonably high. Without field, i.e., $\nu = 1$, the splitting ϵ is only of nonvanishing value if the wall is narrow and/or if $N_A \sim 1$, which means if the system is close to being strictly one dimensional.

VIII. INFLUENCE OF EXTERNAL FIELDS

In this section we show that external fields allow us to control the gauge potential α . In the presence of external fields the four degenerate Bloch wall configurations $\phi_{QC}, \theta = \pi/2$ get deformed into new configurations $\phi(x), \theta(x)$. For moving solitons, $\phi(x-X), \theta(x-X)$, the Berry phase term (2.4) becomes

$$\mathcal{S}_{\text{WZ}} = -i\tilde{\alpha}\tilde{C} \int_0^\beta d\tau \dot{X}, \quad (8.1)$$

where

$$\tilde{\alpha} = \frac{N_A S}{a} \left| \int_{-L/2}^{+L/2} dx \phi'(1 - \cos\theta) \right|, \quad (8.2)$$

and the chirality has been defined as $\tilde{C} = \text{sgn}\{\int dx \phi'(1 - \cos\theta)\}$ with $\phi' = \partial_x \phi$. Note that $\tilde{\alpha}$ is proportional to the area on the unit sphere between the north pole and the trajectory which is traced out by a given spin upon passing of the Bloch wall (cf. Fig. 4). Since the Bloch wall shape changes in response to an applied external field, $\tilde{\alpha}$ will in general differ from the value $\alpha = N_A S \pi/a$ of the Bloch wall ϕ_{QC} , $\theta = \pi/2$.

An external field is taken into account by adding a Zeeman term $g\mu_B \mathbf{B} \cdot \sum_i \mathbf{S}_i$ to the spin Hamiltonian \mathcal{H} (2.1). Correspondingly, the total energy H (2.5) is changed into

$$\tilde{H} = H + N_A \mathbf{h} \cdot \int dx \mathbf{\Omega}, \quad \mathbf{h} = g \frac{\mu_B S}{a} \mathbf{B}. \quad (8.3)$$

For fields along the easy axis or the hard axis, the static configurations satisfy the Euler-Lagrange equations $\delta\tilde{H} = 0$,

$$\begin{aligned} 4J\theta' \phi' \cos\theta + 2J\phi'' \sin\theta + K_y \sin\theta \sin 2\phi \\ + h_x \sin\phi - h_y \cos\phi = 0, \\ -2J\theta'' + \sin 2\theta [J\phi'^2 - K_y \sin^2 \phi - K_z] + h_x \cos\theta \cos\phi \\ + h_y \cos\theta \sin\phi - h_z \sin\theta = 0. \end{aligned} \quad (8.4)$$

We first discuss fields along the hard axis as they have the most interesting effect on the Berry phase. For $h_{x,y} = 0$ but $h_z \neq 0$ all four configurations that emerge from ϕ_{QC} in (3.3) are still energetically degenerate: The invariance of (2.1) under π rotations around the z axis (which remains intact for $h_z \neq 0$) implies the degeneracy of configurations of opposite charge but the same chirality. In addition, states of opposite chirality and charge are also degenerate since with $\phi(x), \theta(x)$ also $-\phi(x), \theta(x)$ solve (8.4) (with $h_{x,y} = 0$).

In the limit of large hard-axis anisotropy, $K_z \gg K_y$, the possible ϕ configurations are still ϕ_{QC} given by (3.3) while

$$\cos\theta = -h_z/K_z. \quad (8.5)$$

Inserting this into (8.2) we have

$$\tilde{\alpha} = \alpha(1 + h_z/K_z), \quad (8.6)$$

which demonstrates that the topological phase (8.1) can indeed be tuned by the external field.

For arbitrary values of the ratio K_z/K_y no analytical solution for the soliton structure can be found. However, we can convince ourselves that $\tilde{\alpha}$ is still field dependent. As is verified by inserting $\phi' = \theta' = 0$ and $\phi = \pm\pi/2$ into (8.4), the spins far away from the soliton get pulled out of the easy plane, $\cos\theta = -h_z/[2(K_y + K_z)]$. Thus in general $\tilde{\alpha}$ is different from α .

How does the field dependence in (8.6) affect the band structure? Let us assume that $\sigma = N_A S d/a$ is a positive integer, i.e., $\tilde{\alpha} \equiv \alpha = \pi\sigma/d$ for $h_z = 0$. The dispersion then has the tight-binding form (6.19) of Fig. 3(a) and consists of two *coinciding* chirality sheets. With increasing field h_z the sheets of opposite chirality $C = \pm$ get separated, each shifted by $\Delta k = |\tilde{\alpha} - \alpha|$. At an external field $h_z^0 = K_z a / 2SN_A d$, this shift becomes $\Delta k = \pi/2d$ and the dispersion shown in Fig. 3(b) is reached. Thus a system with integer σ can be continuously transformed until it reaches half-integer behavior, and vice versa.⁸¹ Note that this behavior is periodic in the field with period $2h_z^0$.⁸² Moreover, if the field $h_z(t)$ and thus

$\tilde{\alpha}(t)$ depends on time, it is clear from the effective Hamiltonian (6.22) that $d\tilde{\alpha}/dt$ plays the role of a force driving the Bloch wall in the positive/negative x direction for positive/negative chirality. Note that this force has its origin in the “classical” part of the Berry phase, $\dot{\phi}\cos\theta$, and therefore can also be deduced from the *classical* Landau-Lifshitz equation (2.7). (It is somewhat surprising that this force, as far as we know, has not been discussed in the literature.)

A similar driving effect is achieved by applying an external field h_y along the easy axis. Indeed, inserting $\phi_{QC}(x-X)$ of Eq. (3.3) into the Zeeman term $h_y \int dx \sin\phi_{QC} = -2h_y N_A Q X$ we see that a weak magnetic field acts like a (classical) force on the soliton center where Q is the charge of the soliton. It can be seen that the phase α remains unaffected by h_y . Note that in analogy to electromagnetism, where $E = -A/c$, h_z plays the role of the vector potential A (albeit chirality dependent), while h_y corresponds to the electric field E . Elsewhere we have discussed in detail^{21,24} how such forces can give rise to Bloch oscillations of the Bloch wall—a magnetic analogue of the Josephson effect. Similarly, we expect a variety of effects for oscillating fields such as resonances due to the Wannier-Stark ladders and related localization effects. Here we just note that external fields along the easy or hard axis can be used to drive the system through the Brillouin zone.

Finally, we consider an external field h_x along the propagation axis. This field lifts the degeneracy between walls of opposite chirality (with Q fixed), and we find from (8.3) $2E_C \equiv \bar{H}[\phi_{Q,C=+}] - \bar{H}[\phi_{Q,C=-}] = 4\pi Q N_A \delta h_x$, which is simply the effective Zeeman splitting energy of the two chirality states. From the exact solutions⁸³ to (8.4) we see that the phase becomes $\tilde{\alpha} = \alpha + C\alpha_0(h_x)$, where α_0 vanishes for $h_x \rightarrow 0$. Hence the relative phase between walls of opposite C remains 2α , independent of the field, and the effective Hamiltonian (6.22) becomes

$$\mathcal{H} = \frac{1}{2M} (p - \alpha\sigma_z)^2 + V(X) + \epsilon\sigma_x + E_C\sigma_z. \quad (8.7)$$

Qualitatively, we see that the last term shifts the dispersion sheets of opposite chirality in opposite *vertical* directions. In the free limit, $V=0$, the eigenvalues are $E_{\pm} = (k^2 + \alpha^2)/2M \pm [k\alpha(k\alpha + 2ME_C)/M^2 + \epsilon^2 + E_C^2]^{1/2}$. Thus the results of Sec. VI remain basically unchanged for $E_C \lesssim \epsilon$ with the level splitting at $k=0$ becoming now $2\sqrt{\epsilon^2 + E_C^2}$. For $E_C > \epsilon$ tunneling of the chirality (as discussed in Sec. VII) and hence its alternation in the Brillouin zone will get suppressed. For instance, if $\epsilon \sim 10$ mK this requires H_x not to exceed 3×10^{-4} Oe (for the YIG values of Sec. VII). On the other hand, the field H_x provides a useful tool to enhance observability of the chirality switching, since it can be used to offset unwanted level detuning and to restore the degeneracy of the chirality states.

Note added in proof. Since submission of the manuscript we have been able to demonstrate that band halving and chirality correlation also occur in the extreme quantum limit of ferromagnetic and antiferromagnetic spin- $\frac{1}{2}$ chains [H.-B. Braun and D. Loss, Int. J. Mod. Phys. B (to be published)]. For antiferromagnetic chains the dispersion is also known as

the “Villain-mode” which has been observed in neutron-scattering experiments [S.E. Nagler *et al.*, Phys. Rev. Lett. **49**, 590 (1982)].

ACKNOWLEDGMENTS

We are grateful to A. S. Arrott and A. J. Leggett for many useful discussions. This work has been supported by the NSERC of Canada and the Swiss NSF (H.B.B.).

APPENDIX A: COHERENT STATES AND BERRY'S PHASE

In this Appendix we discuss the path integrals for coherent spin states⁴⁶ and, in particular, the associated Berry phases. We emphasize single valuedness of spin states and the role of admissible gauges since this is of central importance for the spin parity effects discussed in the main text.

A coherent state is the state of minimal uncertainty for spin components transverse to the spin quantization axis. It is defined as the maximum eigenstate of S_z , $|S, M=S\rangle$, rotated into the direction of the unit vector $\mathbf{\Omega} = (\sin\theta \cos\phi, \sin\theta \sin\phi, \cos\theta)$,

$$|\mathbf{\Omega}\rangle = e^{-iS_z\phi} e^{-iS_y\theta} e^{-iS_x\chi} |S, M=S\rangle, \quad (A1)$$

where \mathbf{S} is the spin operator. By construction, the coherent state (A1) obeys the eigenvalue equation $\mathbf{S} \cdot \mathbf{\Omega} |\mathbf{\Omega}\rangle = S |\mathbf{\Omega}\rangle$ and is an eigenvector of \mathbf{S}^2 with eigenvalue $S(S+1)$. By use of Wigner's formula,⁸⁴ (A1) can be expressed as

$$|\mathbf{\Omega}\rangle = e^{-iS\chi} \sum_{M=-S}^S \binom{2S}{S+M}^{1/2} e^{-iM\phi} \times \left(\cos\frac{\theta}{2} \right)^{S+M} \left(\sin\frac{\theta}{2} \right)^{S-M} |S, M\rangle. \quad (A2)$$

The Euler angle χ has to be fixed by the requirement that the coherent state be *single valued*⁸⁵ upon $\phi \rightarrow \phi + 2\pi n$, $n=0, \pm 1, \dots$. Thus χ is only allowed to take the following values:

$$\chi = (2n+1)\phi, \quad n=0, \pm 1, \dots \quad (A3)$$

For the choices $n=-1$ and $n=0$ we shall use the terms “north-” and “south-pole” gauge, respectively. Of course, the results obtained in either of these gauges must be physically equivalent. Note that this requirement of single valuedness has nothing to do with the transformation properties of $|\mathbf{\Omega}\rangle$ under *active rotations* by 2π which, of course, will always produce a factor of $(-1)^{2S}$ irrespective of the choice of χ .

For later use we list a few important properties^{46,86} of the coherent states (1.2) in the north-pole gauge $\chi = -\phi$. From (1.2) it follows that coherent states are in general not orthogonal,

$$\langle \mathbf{\Omega}' | \mathbf{\Omega} \rangle = \left(\cos\frac{\theta'}{2} \cos\frac{\theta}{2} + \sin\frac{\theta'}{2} \sin\frac{\theta}{2} e^{i(\phi-\phi')} \right)^{2S}, \quad (A4)$$

since $\mathbf{\Omega}$ may vary continuously on the sphere while there are only $2S+1$ mutually orthogonal spin eigenstates. For infinitesimally separated angles, the overlap becomes

$$\langle \mathbf{\Omega}' | \mathbf{\Omega} \rangle = 1 + iS \delta\phi (\cos\theta - 1), \quad (\text{A5})$$

where $\delta\phi = \phi' - \phi$. For the south-pole parametrization $\chi = \phi$, the overlap between infinitesimally separated states becomes

$$\langle \mathbf{\Omega}' | \mathbf{\Omega} \rangle = 1 + iS \delta\phi (\cos\theta + 1). \quad (\text{A6})$$

Coherent states also form an overcomplete set⁴⁶ $[(2S+1)/4\pi] \int d\Omega |\mathbf{\Omega}\rangle \langle \mathbf{\Omega}| = 1$, where $d\Omega = d\phi d(\cos\theta)$. Although the states are not orthogonal, the overlap between different states decreases for rapidly large S with increasing angle, since

$$|\langle \mathbf{\Omega}' | \mathbf{\Omega} \rangle| = \left(\frac{1}{2} (1 + \mathbf{\Omega}' \cdot \mathbf{\Omega}) \right)^S. \quad (\text{A7})$$

In addition we shall make use of the fact that for large S , we have

$$\langle \mathbf{\Omega}' | \mathbf{S} | \mathbf{\Omega} \rangle = [S\mathbf{\Omega} + O(\sqrt{S})] \langle \mathbf{\Omega}' | \mathbf{\Omega} \rangle. \quad (\text{A8})$$

This relation follows from the exact expressions of the spin matrix elements and from the fact that fluctuations have size $O(\sqrt{S})$ since the overlap (1.7) decreases as $\exp\{-S(\mathbf{\Omega}' - \mathbf{\Omega})^2/4\}$.

We derive now a path integral representation for the transition amplitude between two spin configurations. To this end, we represent the state vector of the system as a product of coherent states over all lattice sites $|\{\mathbf{\Omega}\}\rangle = \otimes_{i=1}^{N_L} |\mathbf{\Omega}_i\rangle$. Following the usual procedure,⁴⁶ we slice the interval into N identical pieces of length $\epsilon = \beta/N$ and insert complete sets of states at each lattice site and imaginary time step $\tau_n = n\epsilon$,

$$\begin{aligned} \langle \{\mathbf{\Omega}_b\} | e^{-\beta \mathcal{H}} | \{\mathbf{\Omega}_a\} \rangle \\ = \left(\prod_{m=1}^{N-1} \prod_{i=1}^{N_L} \int d\tilde{\mathbf{\Omega}}_i(\tau_m) \right) \\ \times \prod_{n=0}^{N-1} \langle \{\mathbf{\Omega}(\tau_{n+1})\} | 1 - \epsilon \mathcal{H} | \{\mathbf{\Omega}(\tau_n)\} \rangle, \end{aligned} \quad (\text{A9})$$

where $d\tilde{\mathbf{\Omega}}_i = [(2S+1)/4\pi] d\Omega_i$ and $|\{\mathbf{\Omega}(\tau_0)\}\rangle = |\{\mathbf{\Omega}_a\}\rangle$ and $|\{\mathbf{\Omega}(\tau_N)\}\rangle = |\{\mathbf{\Omega}_b\}\rangle$. In the limit of large S we use (A8) and write

$$\begin{aligned} \langle \{\mathbf{\Omega}(\tau_{n+1})\} | 1 - \epsilon \mathcal{H} | \{\mathbf{\Omega}(\tau_n)\} \rangle \\ = (1 - \epsilon \mathcal{H} [S\mathbf{\Omega}_i(\tau_n)]) \langle \{\mathbf{\Omega}(\tau_{n+1})\} | \{\mathbf{\Omega}(\tau_n)\} \rangle, \end{aligned} \quad (\text{A10})$$

where $\mathcal{H} [S\mathbf{\Omega}_i(\tau_n)]$ is the diagonal element of the Hamiltonian and follows from (2.1) by substituting \mathbf{S}_i by $S\mathbf{\Omega}_i(\tau_n)$. An $O(S^{3/2})$ correction to this diagonal element has been dropped following standard reasoning.² For large S , large deviations between coherent states at adjacent imaginary time steps are exponentially suppressed due to (A7). Therefore the trajectories in imaginary time become smooth, and from (A5) we obtain for the overlap between coherent states at adjacent imaginary time steps

$$\begin{aligned} \langle \{\mathbf{\Omega}(\tau_{n+1})\} | \{\mathbf{\Omega}(\tau_n)\} \rangle \\ = \prod_{i=1}^{N_L} \{ 1 - iS \delta\phi_i(\tau_n) [1 - \cos\theta_i(\tau_n)] \}, \end{aligned} \quad (\text{A11})$$

where $\delta\phi_i(\tau_n) = \phi_i(\tau_{n+1}) - \phi_i(\tau_n)$. These overlap terms are of purely kinematical origin and contribute to (A9) even in the absence of a Hamiltonian. It is these terms which are responsible for the distinct behavior of half-odd-integral and integral spins. Passing to the time continuum limit $N \rightarrow \infty$ we obtain

$$\begin{aligned} \langle \{\mathbf{\Omega}_b\} | e^{-\beta \mathcal{H}} | \{\mathbf{\Omega}_a\} \rangle = \left(\prod_{i=1}^{N_L} \int \mathcal{D}\Omega_i(\tau) \right) \\ \times \exp - \int_0^\beta d\tau \left\{ iS \sum_i \dot{\phi}_i(\tau) \right. \\ \left. \times [1 - \cos\theta_i(\tau)] + \mathcal{H} [S\mathbf{\Omega}_i(\tau)] \right\}, \end{aligned} \quad (\text{A12})$$

where $\mathcal{D}\Omega_i(\tau) = \prod_n \int d\tilde{\mathbf{\Omega}}_i(\tau_n)$ is the measure, and we replaced $\delta\phi_i(\tau)/\epsilon$ by $d\phi_i(\tau)/d\tau$.

In the space continuum limit where the spin configurations vary slowly over the lattice constant a the exchange term in $\mathcal{H} [S\mathbf{\Omega}_i]$ becomes $-\sum_{i,\rho} \mathbf{\Omega}_i \cdot \mathbf{\Omega}_{i+\rho} = \int (d^3r/a) \times \sum_i (\nabla \mathbf{\Omega}_i)^2$. The transition amplitude then takes finally the form

$$\langle \{\mathbf{\Omega}_b\} | e^{-\beta \mathcal{H}} | \{\mathbf{\Omega}_a\} \rangle = \int \mathcal{D}\phi \mathcal{D}(\cos\theta) e^{-\mathcal{S}_E[\phi, \theta]}, \quad (\text{A13})$$

where the path integral runs over configurations that satisfy $\mathbf{\Omega}(x, 0) = \mathbf{\Omega}_a(x)$ and $\mathbf{\Omega}(x, \beta) = \mathbf{\Omega}_b(x)$. The Euclidean action is given by $\mathcal{S}_E = \mathcal{S}_{\text{WZ}} + \int_0^\beta d\tau H$, where the dynamics is determined by the Wess-Zumino or Berry phase term

$$\mathcal{S}_{\text{WZ}} = i \frac{S}{a^3} \int d^3r \int_0^\beta d\tau \dot{\phi} (1 - \cos\theta), \quad (\text{A14})$$

and the energy of the spin configuration is given by

$$\begin{aligned} H = \int \frac{d^3r}{a^3} (\tilde{J} S^2 a^2 [(\nabla\theta)^2 + \sin^2\theta (\nabla\phi)^2] \\ - \tilde{K}_y S^2 \sin^2\theta \sin^2\phi + \tilde{K}_z S^2 \cos^2\theta). \end{aligned} \quad (\text{A15})$$

Equations (A13)–(A15) generalize the formalism of micro-magnetics to include quantum interference effects. Our discussion is not restricted to the anisotropy configurations shown here, one could also include, e.g., magnetostatic interactions of more general form. In the particular case where the spin configuration only depends on one coordinate, we recover (2.2)–(2.5).

Note that the Berry phase term (A14) has been derived in the the north-pole gauge $\chi = -\phi$. If, instead, we had used the south-pole gauge $\chi = \phi$ we would have obtained

$$\mathcal{S}_{\text{WZ}} = -i \frac{S}{a^3} \int d^3r \int_0^\beta d\tau \dot{\phi} (1 + \cos\theta). \quad (\text{A16})$$

This gauge dependence can be traced back to the gauge dependence of the overlap (A5) and (A6) of infinitesimally separated coherent states. It is instructive to express this overlap as a line integral

$$\langle \mathbf{\Omega}'' | \mathbf{\Omega}' \rangle \simeq e^{iS} \int_{\mathbf{\Omega}'}^{\mathbf{\Omega}''} d\mathbf{\Omega} \cdot \mathbf{A}_{N,S} \quad (\text{A17})$$

over a “vector potential” $\mathbf{A}_{N,S} = \mathbf{e}_\phi (\cos\theta \mp 1) / \sin\theta$, where the upper (lower) sign corresponds to the north- (south-) pole parametrization. These vector potentials⁸⁷ are equivalent to that of a magnetic monopole of unit strength evaluated on the surrounding unit sphere. The gauge character of the different parametrizations of the coherent state (A1) now becomes apparent. If we gauge transform the coherent state $|\mathbf{\Omega}\rangle \mapsto e^{-i\Lambda} |\mathbf{\Omega}\rangle$, where $\Lambda = \lambda \phi$, the overlap (A17) transforms according to $\mathbf{A} \mapsto \mathbf{A} + \nabla_\phi \Lambda$. By the choice of the gauge one decides whether a part of the Berry phase “disappears” in the definition of the coherent state or whether it appears explicitly in the path integral via the overlap (A17). However, in order to preserve the single valuedness of the coherent states—our fundamental postulate—only gauge transformations $\exp\{-i\Lambda\}$ are admissible^{88,69} that are single valued upon $\phi \rightarrow \phi + 2\pi$. Evidently, this is the case for $\Lambda = 2S\phi$ (for all S) which relates the north- and south-pole parametrizations. On the other hand, for half-odd-integer spin this condition is violated for $\Lambda = S\phi$ which relates the coherent state with $\chi = -\phi$ to the one with $\chi = 0$, but the latter is not single valued and thus not an admissible state. The corresponding vector potential would be $\mathbf{A}_0 = -\cot\theta \mathbf{e}_\phi$ and does not yield the full Berry phase accumulated in a closed circuit: $\oint d\mathbf{\Omega} \cdot \mathbf{A}_0$ measures the area between the trajectory on the unit sphere and the equator while $\oint d\mathbf{\Omega} \cdot \mathbf{A}_{N,S}$ measures the area between the trajectory and the north or south pole. For trajectories crossing the dateline⁵⁰ (this is typically the case if spherical coordinates are chosen that are adapted to the symmetry of the Hamiltonian), the phase factor $\exp\{iS \oint d\mathbf{\Omega} \cdot \mathbf{A}_0\}$, that results from the “wrong” choice $\chi = 0$ for the coherent state (A1), *does not* coincide with the Berry phase term, $\exp\{iS \oint d\mathbf{\Omega} \cdot \mathbf{A}_{N,S}\}$, for half-odd-integer spins and would, e.g., lead to a wrong semiclassical spin quantization.

APPENDIX B: EVALUATION OF THE DAMPING KERNEL

In this Appendix we present the derivation of the damping kernel (5.15) starting from Eq. (5.8).

In order to evaluate F in (5.8) we first complete the square in the exponential. As we are working only to order $O(\dot{X}^2/c^2)$, it is sufficient to shift φ by $\rho \equiv (1/2)\mathcal{S}^{-1}\mathcal{J}$ since

$$\varphi \cdot [\mathcal{S} + \mathcal{K}] \varphi + \mathcal{J} \cdot \varphi = (\varphi + \rho) \cdot [\mathcal{S} + \mathcal{K}] (\varphi + \rho) + O(\dot{X}^3) \quad (\text{B1})$$

(\mathcal{S} and \mathcal{K} are Hermitian). Thus Eq. (5.8) can be rewritten as

$$F[X] = \int \mathcal{D}\tilde{\varphi} \det \left[\int dx \{ \phi_0'^2 - \phi_0'' [\tilde{\varphi} - \rho] \} \delta(\tau - \tau') \right] \times \delta \left(\int \phi_0' [\tilde{\varphi} - \rho] \right) e^{-N_A \tilde{\varphi} \cdot [\mathcal{S} + \mathcal{K}] \tilde{\varphi}}, \quad (\text{B2})$$

where $\tilde{\varphi} = \varphi + \rho$. Equation (B2) can now be considerably simplified. First we note that $\int dx \phi_0' \rho \propto \int dx \phi_0' \mathcal{S}^{-1} \phi_0'' = 0$ due to the parity invariance of \mathcal{S} and (anti)symmetry of ϕ_0' (ϕ_0''). Thus the δ function enforces $\tilde{\varphi}$ to be orthogonal to the zero mode. The Gaussian integrations over $\tilde{\varphi}$ are then well

defined and the fluctuations have effective size $O(1/\sqrt{N_A})$. Rescaling $\hat{\varphi} = \sqrt{N_A} \tilde{\varphi}$ and making use of the identity $\det = \exp \text{tr} \ln$, we can rewrite $\det(\delta Q / \delta X)$ as

$$\exp \left\{ \text{tr} \ln \left(1 - \frac{\delta/2}{\sqrt{N_A}} \int \phi_0'' \hat{\varphi} + (\delta/2) \int \phi_0'' \rho \right) \right\}, \quad (\text{B3})$$

where we used $\int \phi_0'^2 = 2/\delta$ [cf. (3.5)], and where the constant $\exp\{\text{tr} \ln(2/\delta)\}$ has been absorbed into the integration measure. The second term under the logarithm can be neglected for large N_A and the last term being proportional to \dot{X}^2 gives rise to a pure mass renormalization. Neglecting irrelevant prefactors, Eq. (2.2) thus becomes

$$F[X] = e^{-(\Delta M/2) \int d\tau \dot{X}^2} \int \mathcal{D}\hat{\varphi} \delta \left(\int \phi_0' \hat{\varphi} \right) e^{-\hat{\varphi} \cdot [\mathcal{S} + \mathcal{K}] \hat{\varphi}} = e^{-(\Delta M/2) \int d\tau \dot{X}^2} \frac{1}{\sqrt{\det'(\mathcal{S} + \mathcal{K})}}, \quad (\text{B4})$$

where the prime on the determinant denotes omission of the zero mode which is enforced by the δ function, and $\Delta M = O((N_A)^0)$ is a small mass renormalization whose exact value is not of interest here. In the evaluation of the determinant we will encounter several (ultraviolet) divergent terms which also have the form of a mass renormalization of order $O((N_A)^0)$. All these renormalizations will change the mass M into the experimentally observed “dressed” Bloch wall mass M_{eff} . We will thus drop all these renormalization terms and simply replace $M \rightarrow M_{\text{eff}}$ in the action (5.7).

Moreover, since the SG model is known to be renormalizable⁷¹ and since we are interested only in the long time (infrared) behavior there is no need here to carry out a systematic renormalization procedure to remove the short time divergences.

We now turn to the explicit evaluation of the determinant in (B4). We make again use of the identity $\ln \det = \text{tr} \ln$ and expand the logarithm:

$$\begin{aligned} & \frac{1}{\sqrt{\det'(\mathcal{S} + \mathcal{K})}} \\ &= e^{-(1/2) \text{tr}' \ln(\mathcal{S}[1 + \mathcal{S}^{-1}\mathcal{K}])} \\ &= \frac{1}{\sqrt{\det' \mathcal{S}}} e^{-(1/2) \text{tr}' [\mathcal{S}^{-1}\mathcal{K} - (1/2)\mathcal{S}^{-1}\mathcal{K}\mathcal{S}^{-1}\mathcal{K} + O(\dot{X}/c^3)]}. \end{aligned} \quad (\text{B5})$$

Since $\mathcal{K} = O(\dot{X}/c)$ this represents an expansion in increasing powers of \dot{X}/c . The factor $[\det' \mathcal{S}]^{-1/2}$ is independent of \dot{X} and is the partition function of spin wave fluctuations around the static Bloch wall. The trace in (B5), $\text{tr}(\cdots) = \sum_{\mathbf{k}} \langle \mathbf{k} | \cdots | \mathbf{k} \rangle$, is evaluated in the basis of eigenfunctions of \mathcal{S} ,

$$\mathcal{S} | \mathbf{k} \rangle = \epsilon_{\mathbf{k}} | \mathbf{k} \rangle, \quad \epsilon_{\mathbf{k}} = Jk^2 + \kappa \omega^2 + K_y, \quad (\text{B6})$$

where $\kappa = J/c^2$. The anisotropy gap K_y will have important consequences for the form of the damping kernel below. The eigenfunctions factorize into a space and (imaginary) time

part, $|\mathbf{k}\rangle = |\omega\rangle|k\rangle$, where $\langle\tau|\omega\rangle = e^{i\omega\tau}/\sqrt{\beta}$ with Matsubara frequencies $\omega = 2\pi\nu/\beta$, $\nu = 0, \pm 1, \dots$. Since the contribution of the zero mode ϕ_0' is explicitly excluded in (B5), we only need the spin wave states^{43,44}

$$\langle x|k\rangle = N_k[-ik\delta + \tanh(x/\delta)]e^{ikx}, \quad (\text{B7})$$

where $N_k = [L(1+k^2\delta^2)]^{-1/2}$. The k values in (B7) are implicitly defined by

$$kL + \Delta(k) = 2\pi n, \quad (\text{B8})$$

where $\Delta(k) = 2\arctan 1/k\delta$ is the scattering phase shift of the eigenfunction (B7).

To render the results finite in the thermodynamic limit, we have to subtract the vacuum fluctuations⁶³ and thus renormalize,

$$\frac{1}{\det'(\mathcal{S} + \mathcal{H})} \rightarrow \frac{\det(\mathcal{S}_0 + \mathcal{H})}{\det'(\mathcal{S} + \mathcal{H})}, \quad (\text{B9})$$

where $\mathcal{S}_0 = -\kappa\partial_\tau^2 - J\partial_x^2 + K_y$ is the operator describing spin waves around the anisotropy minimum in the absence of a Bloch wall. \mathcal{S}_0 has the *same* eigenvalues (B6) as \mathcal{S} but the space eigenfunctions are simply plane waves where the k values are given by $k_{\text{free}} = 2\pi n/L$ rather than (B8). For the results given below which only involve one summation over k , the renormalization (B9) then simply amounts to the replacement

$$\sum_k \rightarrow \sum_k - \sum_{k_{\text{free}}} = \int_{-\infty}^{\infty} dk [\rho(k) - \rho_{\text{free}}] = \int_{-\infty}^{\infty} \frac{dk}{2\pi} \frac{d\Delta}{dk}, \quad (\text{B10})$$

where $\rho = dn/dk = L/2\pi - (1/2\pi)(d\Delta/dk)$ is the density of states corresponding to (B8), $\rho_{\text{free}} = 2\pi/L$, and where we go over now to the thermodynamic limit. From the definition of Δ it follows that $d\Delta/dk = -2\delta/(k^2\delta^2 + 1)$.

With these preliminaries, we can now rewrite the lowest-order term in (B5) as follows:

$$\begin{aligned} -\frac{1}{2}\text{tr}\mathcal{S}^{-1}\mathcal{H} &= -\frac{1}{2}\sum_{\mathbf{k}} \frac{\kappa}{\epsilon_{\mathbf{k}}} [2\langle k|-i\partial_x|k\rangle\langle\omega|i\dot{X}\partial_\tau|\omega\rangle \\ &\quad - \langle k|\partial_x^2|k\rangle\langle\omega|\dot{X}^2|\omega\rangle], \end{aligned} \quad (\text{B11})$$

where $\kappa = J/c^2$. Using the eigenfunctions (B7) we obtain $\langle k|-i\partial_x|k'\rangle = k\delta_{kk'} + O(L^{-1})$ and $\langle k|\partial_x^2|k'\rangle = -k^2\delta_{kk'} + O(L^{-1})$. Inserting the identity $1 = \int d\tau|\tau\rangle\langle\tau|$ we obtain in leading order in L

$$-\frac{1}{2}\text{tr}\mathcal{S}^{-1}\mathcal{H} = \frac{\kappa}{2\beta}\sum_{\mathbf{k}} \frac{k}{\epsilon_{\mathbf{k}}}\int d\tau\{2\omega\dot{X} - k\dot{X}^2\}. \quad (\text{B12})$$

The first term on the RHS vanishes since $\epsilon_{\mathbf{k}}$ is symmetric in both k and ω and the second term leads to a mass renormal-

ization which diverges logarithmically [after the partial renormalization (B10)]. As mentioned above, this term is part of the dressing of the ‘‘bare’’ Döring mass to the experimentally observed value M_{eff} , and thus there is no need to remove this divergence explicitly.

The damping due to spin waves will be exclusively due to the remaining terms in (B5) which will be discussed next. Using the above notation, we have up to order \dot{X}^2

$$\frac{1}{4}\text{tr}(\mathcal{S}^{-1}\mathcal{H})^2 = \kappa^2\sum_{\mathbf{k},\mathbf{k}'} \frac{1}{\epsilon_{\mathbf{k}}\epsilon_{\mathbf{k}'}} |\langle\mathbf{k}|\dot{X}\partial_\tau\partial_x|\mathbf{k}'\rangle|^2. \quad (\text{B13})$$

In leading order in L we have

$$\langle\mathbf{k}|\dot{X}\partial_\tau\partial_x|\mathbf{k}'\rangle = -\frac{k\omega'}{\beta}\delta_{kk'}\int d\tau e^{i(\omega' - \omega)\tau}\dot{X}(\tau). \quad (\text{B14})$$

Thus Eq. (B13) can be rewritten in the form

$$\frac{1}{4}\text{tr}(\mathcal{S}^{-1}\mathcal{H})^2 = \int_0^\beta d\tau \int_0^\beta d\sigma \dot{X}(\tau)\dot{X}(\sigma)\gamma(\tau - \sigma), \quad (\text{B15})$$

with

$$\gamma(\tau) = \frac{1}{\beta^2}\sum_{\omega,\omega',k} \frac{k^2\omega\omega' e^{i(\omega' - \omega)\tau}}{[\omega^2 + \omega_k^2][\omega'^2 + \omega_k^2]}, \quad (\text{B16})$$

where $\omega_k^2 = c^2(k^2 + \delta^{-2})$. With partial integrations and with $\gamma(\tau + \beta) = \gamma(\tau)$ Eq. (B15) reduces to

$$\frac{1}{4}\text{tr}(\mathcal{S}^{-1}\mathcal{H})^2 = -\frac{1}{2}\int_0^\beta d\tau \int_0^\tau d\sigma K(\tau - \sigma)[X(\tau) - X(\sigma)]^2, \quad (\text{B17})$$

where $K(\tau) = -2\partial_\tau^2\gamma$. In (B17), we have neglected a term $2[X(\beta) - X(0)]\int d\tau\dot{X}\gamma$ which turns out to be small for typical tunneling processes. For the evaluation of γ and K we make use of the exact relation

$$D_\omega(\tau) = \frac{2\omega}{\beta}\sum_{n=-\infty}^{\infty} \frac{e^{i\omega_n\tau}}{\omega_n^2 + \omega^2} = \frac{\cosh[\omega(|\tau| - \beta/2)]}{\sinh(\beta\omega/2)}, \quad (\text{B18})$$

where $\omega_n = 2\pi n/\beta$ and the RHS is understood to be periodically extended beyond $|\tau| \leq \beta/2$. With (B16) and (B18) we finally obtain for $K = -2\partial_\tau^2\gamma$

$$K(\tau) = \sum_{\mathbf{k}} k^2\omega_k^2 \left[\sinh^{-2}\left(\frac{\beta\omega_k}{2}\right) - 2D_{\omega_k}^2(\tau) \right]. \quad (\text{B19})$$

Note that as a consequence of the relevant coupling between the system \dot{X} and the bath which is quadratic in the bath coordinates φ , K is proportional to D_ω^2 rather than D_ω as in the usual Caldeira-Leggett theory. For low temperatures, the damping kernel (B19) reduces to $K(\tau) = -2\sum_{\mathbf{k}} k^2\omega_k^2 e^{-2\omega_k|\tau|}$.

- ¹M. V. Berry, Proc. R. Soc. London Ser. A **392**, 45 (1984).
- ²F. D. M. Haldane, Phys. Rev. Lett. **50**, 1153 (1983).
- ³I. Affleck, J. Phys. Condens. Matter. **1**, 3047 (1989).
- ⁴D. Loss and D. L. Maslov, Phys. Rev. Lett. **74**, 178 (1995).
- ⁵See, e.g., *Magneto-electronics*, Special issue of Phys. Today **48**(4) (1995).
- ⁶*Quantum Tunneling in Magnetism*, Proceedings of the NATO Conference, edited by B. Barbara and L. Gunther (Kluwer, Dordrecht, The Netherlands, 1995).
- ⁷M. Enz and R. Schilling, J. Phys. C **19**, 1765 (1986); **19**, L711 (1986).
- ⁸J. L. van Hemmen and S. Sütö, Europhys. Lett. **1**, 481 (1986).
- ⁹E. M. Chudnovsky and L. Gunther, Phys. Rev. Lett. **60**, 661 (1988); Phys. Rev. B **37**, 9455 (1988).
- ¹⁰A. Garg and G. H. Kim, Phys. Rev. B **45** 12 921 (1992).
- ¹¹B. Barbara and E. M. Chudnovsky, Phys. Lett. A **145**, 205 (1990); I. Krive and O.B. Zaslavskii, J. Phys. Condens. Matter **2**, 9457 (1990).
- ¹²C. Paulsen *et al.*, Phys. Lett. A **161**, 319 (1991).
- ¹³W. Wernsdorfer *et al.*, J. Magn. Magn. Mater. **145**, 1 (1995).
- ¹⁴For a critical discussion of relaxation measurements, see E. Vincent *et al.*, J. Phys. (France) I **4**, 273 (1994).
- ¹⁵D. D. Awschalom, J. F. Smyth, G. Grinstein, D. P. DiVincenzo, and D. Loss, Phys. Rev. Lett. **68**, 3092 (1992); **71**, 4279(E) (1993).
- ¹⁶S. Gider, D. D. Awschalom, T. Douglas, and S. Mann, Science **268**, 77 (1995); see also D. D. Awschalom and D. P. DiVincenzo, Phys. Today **48**(4), 43 (1995).
- ¹⁷A. Garg, Phys. Rev. Lett. **70**, 2198 (1993); **71**, 4249 (1993); **74**, 1458 (1995); see also D. D. Awschalom, J. F. Smyth, G. Grinstein, D. P. DiVincenzo, and D. Loss, Phys. Rev. Lett. **70**, 2199 (1993); **71**, 4276 (1993).
- ¹⁸D. Loss, D. DiVincenzo, and G. Grinstein, Phys. Rev. Lett. **69**, 3233 (1992).
- ¹⁹J. van Delft and C. Henley, Phys. Rev. Lett. **69**, 3237 (1992).
- ²⁰D. Loss, D. P. DiVincenzo, G. Grinstein, D. D. Awschalom, and J. F. Smyth, Physica B **189**, 189 (1993).
- ²¹H. B. Braun and D. Loss, Europhys. Lett. **31**, 555 (1995); in *Quantum Tunneling in Magnetism* (Ref. 6).
- ²²E. M. Chudnovsky, J. Magn. Magn. Mater. **140-144**, 1821 (1995).
- ²³J. M. Duan and A. Garg, J. Phys. Condens. Matter **7**, 2171 (1995).
- ²⁴H. B. Braun and D. Loss, J. Appl. Phys. **76**, 6177 (1994).
- ²⁵For an experimental realization of such a ferromagnetic grating in semiconductors see, e.g., P. D. Ye *et al.*, Phys. Rev. Lett. **74**, 3013 (1995).
- ²⁶M. Uehara and B. Barbara, J. Phys. (Paris) **47**, 235 (1987); B. Barbara *et al.*, J. Appl. Phys. **73**, 6703 (1993).
- ²⁷K. Hong and N. Giordano, in *Quantum Tunneling in Magnetism* (Ref. 6).
- ²⁸T. Egami, Phys. Status Solidi B **57**, 211 (1973); Phys. Status Solidi A **19**, 747 (1973); **20**, 157 (1973).
- ²⁹W. Riehemann and E. Nembach, J. Appl. Phys. **55**, 1081 (1984).
- ³⁰P. C. E. Stamp, Phys. Rev. Lett. **66**, 2802 (1991).
- ³¹P. C. E. Stamp, E. M. Chudnovsky, and B. Barbara, Int. J. Mod. Phys. B **6**, 1355 (1992).
- ³²G. Tatara and H. Fukuyama, Phys. Rev. Lett. **72**, 772 (1994); J. Phys. Soc. Jpn. **63**, 2538 (1994).
- ³³The treatment of the general case is more involved but still possible; the results are similar in nature and will be presented elsewhere (Ref. 34).
- ³⁴H. B. Braun and D. Loss (unpublished).
- ³⁵A. O. Caldeira and A. J. Leggett, Ann. Phys. (N.Y.) **149**, 347 (1983).
- ³⁶U. Weiss, *Quantum Dissipative Systems* (World Scientific, Singapore, 1993).
- ³⁷See A. J. Leggett, *Quantum Tunneling in Condensed Media* (North-Holland, Amsterdam, 1992).
- ³⁸J. F. Janak, Phys. Rev. **134**, A411 (1964).
- ³⁹A. S. Abyzov and B. A. Ivanov, Zh. Éksp. Teor. Fiz. **76**, 1700 (1979) [Sov. Phys. JETP **49**, 865 (1979)].
- ⁴⁰B. A. Ivanov, A. K. Kolezhuk, and Yu. N. Mitsai, Fiz. Nizk. Temp. **16**, 1412 (1990) [Sov. J. Low Temp. Phys. **16**, 800 (1991)].
- ⁴¹V. G. Bar'yakhtar and B. A. Ivanov, Sov. Sci. Rev. A **16**, 1 (1992).
- ⁴²A. H. Castro Neto and A. O. Caldeira, Phys. Rev. B **46**, 8858 (1992); Phys. Rev. E **48**, 4037 (1993).
- ⁴³H. B. Braun, Phys. Rev. B **50**, 16 485 (1994).
- ⁴⁴J. M. Winter, Phys. Rev. **124**, 452 (1962).
- ⁴⁵The lowest-energy spin wave modes are the Winter modes (Refs. 44,38) with dispersion $\epsilon_{\mathbf{k}} = (2\sqrt{Ja/S})k\sqrt{J\mathbf{k}^2 + K_z}$ where $\mathbf{k} = (k_y, k_z)$ is the wave vector transverse to the sample axis. These modes are gapless for an infinite sample but they acquire a finite size gap for a mesoscopic sample since the minimal wave vector component is $k_{\min} = \pi/w$, where w is the maximal transverse width. Thus the spin waves are frozen out for $k_B T < \epsilon_{\mathbf{k}}$, or equivalently if at temperature T the sample width is smaller than $w_0(T) = \pi\sqrt{2J/K_z}[\sqrt{1 + \tau^2} - 1]^{-1/2}$ with $\tau = k_B T S / K_z a$. Note that w_0 increases with decreasing temperature, e.g., for YIG with parameters as in Sec. VII, we have $w_0 = 400 \text{ \AA}$ at $T = 0.5 \text{ K}$, while at $T = 50 \text{ mK}$ we have $w_0 = 2800 \text{ \AA}$.
- ⁴⁶J. Klauder, Phys. Rev. D **19**, 2349 (1979).
- ⁴⁷A. P. Malozemoff and J. C. Slonczewski, *Magnetic Domain Walls in Bubble Materials* (Academic, New York, 1979).
- ⁴⁸W. F. Brown, *Micromagnetics* (Interscience Publishers, New York, 1963).
- ⁴⁹J. F. Dillon, in *Magnetism*, edited by G. R. Rado and H. Suhl (Academic, New York, 1963), Vol. III, and references therein.
- ⁵⁰A. Auerbach, *Interacting Electrons and Quantum Magnetism* (Springer, New York, 1994), Chap. 10.
- ⁵¹H.-J. Mikeska and M. Steiner, Adv. Phys. **40**, 191 (1991).
- ⁵²Note that on-site anisotropies are ineffective for $S = 1/2$. On the other hand, exchange anisotropy supports the existence of ferromagnetic solitons also in this case (see, e.g., Ref. 51), and thus Eq. (2.3) may be regarded as an effective model for such soliton excitations even for $S = 1/2$.
- ⁵³At this point we reduce the topology of the two-sphere S^2 to the S^1 topology of the spin confined to the easy plane. In Sec. VI D we shall consider what happens if the soliton can tunnel between two chiralities, which belong to two distinct topological sectors of the sine-Gordon field configuration.
- ⁵⁴U. Enz, Helv. Phys. Acta **37**, 245 (1964).
- ⁵⁵In micromagnetic notation this reads $\omega = 2(\gamma/M_0) \times ([Ak^2 + K_e + K_h][Ak^2 + K_e])^{1/2}$, where A, K_e , and K_h are defined as in Sec. II, and $\gamma/M_0 = a^3/\hbar S$.
- ⁵⁶H. B. Braun and O. Brodbeck, Phys. Rev. Lett. **70**, 3335 (1993).
- ⁵⁷Note, however, that high-energy soliton-soliton breather solutions of Ref. 56 do not have a counterpart in the sine-Gordon model.
- ⁵⁸This notation differs from that of Ref. 18. Denoting the (positive) anisotropy constants of the latter work by \vec{K}_y and \vec{K}_z , we have $\vec{K}_y = (a/NS^2)K_y$ and $\vec{K}_z = (a/NS^2)(K_y + K_z)$.

- ⁵⁹R. Rajaraman, *Solitons and Instantons* (North-Holland, Amsterdam, 1982).
- ⁶⁰For a perturbative tunnel splitting calculation, see also I. Ya. Korenblit and E. F. Shender, *Sov. Phys. JETP* **48**, 937 (1978).
- ⁶¹See R. F. Dashen, B. Hasslacher, and A. Neveu, *Phys. Rev. D* **12**, 3424 (1975), for the quantization of a *static* soliton. In this case, no special treatment is needed for the Goldstone mode.
- ⁶²J.-L. Gervais and B. Sakita, *Phys. Rev. D* **11**, 2934 (1975).
- ⁶³B. Sakita, *Quantum Theory of Many Variable Systems and Fields* (World Scientific, Singapore, 1985).
- ⁶⁴Note that the boundary conditions on the field ϕ (which contains a Bloch wall) ensure that Q has indeed a zero: since $\phi'_0(x)$ is a localized positive function, the sign of Q will be proportional to the sign of ϕ which changes at least once as a function of x due to the boundary conditions.
- ⁶⁵H. B. Braun, *Phys. Rev. Lett.* **71**, 3557 (1993); *Phys. Rev. B* **50**, 16 501 (1994).
- ⁶⁶Equation (5.17) differs from previous investigations [cf. (4.41) of Ref. 31] which obtain *gapless* spectral functions of the "Ohmic type," i.e., $J(\omega) \propto \omega$. This can be partly traced back to their use (Ref. 31) of massless Winter modes; however, see Ref. 45.
- ⁶⁷The strength V_0 of the pinning potential can be related to a classical coercivity via $V_0/\mathcal{A} = H_c M_0 d/\pi$ where \mathcal{A} is the sample cross sectional area. H_c is defined as the field H at which the force $2\mathcal{A}M_0H$ on the domain wall due to the external field renders the potential $V(X)$ unstable.
- ⁶⁸In a finite system, strictly speaking, periodic boundary conditions correspond physically to a ring geometry which would require a pair of π Bloch walls. However, in the thermodynamic limit the Bloch walls can be separated far enough from each other so that we may treat them independently.
- ⁶⁹D. Loss and P. M. Goldbart, *Phys. Rev. B* **45**, 13 544 (1992); D. Loss, H. Schoeller, and P. M. Goldbart, *ibid.* **48**, 15 218 (1993).
- ⁷⁰Note that this is quite different from, e.g., a persistent current, where the counterpart of α , the Aharonov-Bohm flux, scales inversely proportionally to the sample length at constant field. See also Sec. VI D.
- ⁷¹J. Zinn-Justin, *Quantum Field Theory and Critical Phenomena* (Oxford University Press, New York, 1993).
- ⁷²The period halving is directly seen if, instead, we choose vanishing boundary conditions. In this case we may perform a gauge transformation on (6.4) with $e^{-i\alpha X \sigma_z} \mathcal{H} e^{i\alpha X \sigma_z} = p^2/2M + \epsilon \sigma_x \cos(2\alpha X) + \epsilon \sigma_y \sin(2\alpha X) + V(X)$, which leaves the partition function unaltered. Thus the induced space potential has now double the period, $2d$ (with interchanged chiralities), which translates into half the period in reciprocal space. Note that this argument cannot be used for periodic boundary conditions, since the wave functions in the new gauge are no longer periodic.
- ⁷³H. J. Ziman, *Principles of the Theory of Solids*, 2nd ed. (Cambridge University Press, Cambridge, England, 1972).
- ⁷⁴M. Büttiker, I. Imry, and R. Landauer, *Phys. Lett.* **96A**, 365 (1983).
- ⁷⁵See, e.g., P. G. deGennes, *Superconductivity of Metals and Alloys* (W. A. Benjamin, Inc., New York, 1966).
- ⁷⁶D. J. Thouless and Y. Gefen, *Phys. Rev. Lett.* **66**, 806 (1991).
- ⁷⁷N. Byers and C. N. Yang, *Phys. Rev. Lett.* **7**, 46 (1961).
- ⁷⁸R. S. Tebble and D. J. Craik, *Magnetic Materials* (Wiley-Interscience, New York, 1969), p. 313.
- ⁷⁹T. H. O'Dell, *Ferromagnetodynamics* (Macmillan, London, 1981), p. 65.
- ⁸⁰This value of the coercivity is an empirical value since no data are known for sufficiently small YIG samples at the temperatures of interest. For macroscopic samples, coercivities as low as 10^{-2} Oe are reported (Ref. 49). Since the coercivity is expected to increase with decreasing sample size and temperature, we assume a coercivity of 2 Oe.
- ⁸¹This effect is again gauge independent. In an arbitrary gauge (A3) we have $\tilde{\alpha}_n = (\sigma/d) \int d\phi ([2n+1] - \cos\theta) = \tilde{\alpha} + nC\sigma 2\pi/d$ since ϕ_{QC} flips the spins by $C\pi$. Thus the positive and negative chirality branches are each shifted by a reciprocal lattice vector (or half a reciprocal lattice vector for σ half integer). Hence for integer and half-integer σ the spectra obtained in different gauges merely differ by multiples of a reciprocal lattice vector $2\pi/d$ and thus are identical.
- ⁸²For spatially uniform configurations the phase (8.6) reduces to $NS\pi(1 + h_z/K_z)$. Inserting this into the cosine of (4.12) we see that the tunnel splitting oscillates with the field. See also A. Garg, *Europhys. Lett.* **22**, 205 (1993).
- ⁸³R. M. Hornreich and H. Thomas, *Phys. Rev.* **17**, 1406 (1978).
- ⁸⁴J. J. Sakurai, *Modern Quantum Mechanics* (Addison-Wesley, Reading, MA, 1994), Chap. 3.8.
- ⁸⁵This is analogous to the use of a locally *single valued* basis $|n(\mathbf{R})\rangle$ in the expression $\gamma_n = i \oint d\mathbf{R} \cdot \langle n(\mathbf{R}) | \nabla_{\mathbf{R}} | n(\mathbf{R}) \rangle$ for the Berry phase (Refs. 1,69). Note, however, that the present derivation does not make use of an adiabatic approximation.
- ⁸⁶See, e.g., T. Einarsson and H. Johannesson, *Phys. Rev. B* **43**, 5867 (1991).
- ⁸⁷ \mathbf{A}_N exhibits a Dirac-string singularity through the south and \mathbf{A}_S through the north pole. These singularities reflect the fact that there is no globally unique parametrization for the coherent states. For $\chi = -\phi$ the coherent state (A1) takes the ambiguous form $|\mathbf{\Omega}\rangle = \exp\{2iS\phi\}|S,S\rangle$ at $\theta = \pi$ and a similar ambiguity holds for the parametrization $\chi = \phi$ at the north pole $\theta = 0$.
- ⁸⁸T. T. Wu and C. N. Yang, *Phys. Rev. D* **12**, 3845 (1975).